

Mean-field-game approach to nonpharmaceutical interventions in a social-structure model of epidemics

Louis Bremaud ^{1,*}, Olivier Giraud ^{1,2,3} and Denis Ullmo ¹

¹*Université Paris-Saclay, CNRS, LPTMS, 91405 Orsay, France*

²*MajuLab, CNRS-UCA-SU-NUS-NTU International Joint Research Unit, Singapore*

³*Centre for Quantum Technologies, National University of Singapore, Singapore*

 (Received 26 April 2024; accepted 7 November 2024; published 2 December 2024)

The design of coherent and efficient policies to address infectious diseases and their consequences requires modeling not only epidemics dynamics but also individual behaviors, as the latter has a strong influence on the former. In our work, we provide a theoretical model for this problem, taking into account the social structure of a population. This model is based on a mean-field-game version of a SIR compartmental model, in which individuals are grouped by their age class and interact together in different settings. This social heterogeneity allows us to reproduce realistic situations while remaining usable in practice. In our game theoretical approach, individuals can choose to limit their contacts by making a trade-off between the risks incurred by infection and the cost of being confined. The aggregation of all these individual choices and optimizations forms a Nash equilibrium through a system of coupled equations that we derive and solve numerically. The global cost born by the population within this scenario is then compared to its societal optimum counterpart (i.e., the cost associated with the optimal set of strategies from the point of view of the society as a whole), and we investigate how the gap between these two costs can be partially bridged within a *constrained Nash equilibrium* for which a governmental institution would, under specific conditions, impose “partial lockdowns” such as the ones that were imposed during the COVID-19 pandemic. Finally, we consider the consequences of the finiteness of the population size N_{tot} , or of a time T at which an external event (e.g., a vaccine) would end the epidemic, and show that the variation of these parameters could lead to *first-order phase transitions* in the choice of optimal strategies. In this paper, all the strategies considered to mitigate epidemics correspond to nonpharmaceutical interventions, and we provide here a theoretical framework within which guidelines for public policies depending on the characteristics of an epidemic and on the cost of restrictions on the society could be assessed.

DOI: [10.1103/PhysRevE.110.064301](https://doi.org/10.1103/PhysRevE.110.064301)

I. INTRODUCTION

As our history with COVID-19 has made rather explicit, modeling as precisely as possible the dynamics of epidemics is crucial if one wishes to design public policies able to mitigate effectively their negative impact. One major difficulty encountered toward this goal is that, most often, the parameters one would naturally choose to build such models have significant, and sometimes very fast, variations. This is illustrated, for instance, by the graph plotted in Fig. 1, which shows the time dependence of R_{eff} , the average number of people to which the virus is transmitted by a sick individual, for the COVID-19 pandemic in France.

The figure reveals that there are huge variations of R_{eff} over time. Some of them can easily be associated with known events (lockdown, new variant, etc.) but some other remain unexplained. Indeed, R_{eff} is impacted by many phenomena, such as natural immunity, vaccination, but also by behavioral changes that have important consequences on the spreading of the disease. While data such as immunity or vaccination rate are taken into account in even the most basic models, this is not the case for the evolution of social interactions.

However, these modifications of social behavior, either under governmental influence or because people change their individual habits, significantly affect epidemics dynamics. These individual or collective strategies against the virus sometimes prevented a health disaster [1] by significantly decreasing the total number of infected people and the time at which the peak occurs [1,2]. As a counterpart, they had significant worldwide negative impact, for the economy [3], or in terms of health (as medical acts had to be postponed), time, money, social interactions, psychological pressure [4] (domestic violence, depression), etc., which in turn could increase the stress on the sanitary system [2]. In such a context, any policy or any individual decision must consider the trade-off between the cost of reducing social interaction and the cost of the epidemic; see, for instance, Refs. [5–7], where realistic impacts and constraints on the quarantine and isolation strategies have been considered, and Refs. [8,9] where the individual behavioral response to isolation policy has been investigated. This individual response is of course greatly influenced by cultural habits together with social, economic, religious needs of the population.

In models currently used to describe the propagation of epidemics, social interactions are often described by constant parameters, or at best by time-dependent parameters which are *extrinsic*, in the sense that their time evolution is not predicted

*Contact author: louis.bremaud@hotmail.fr

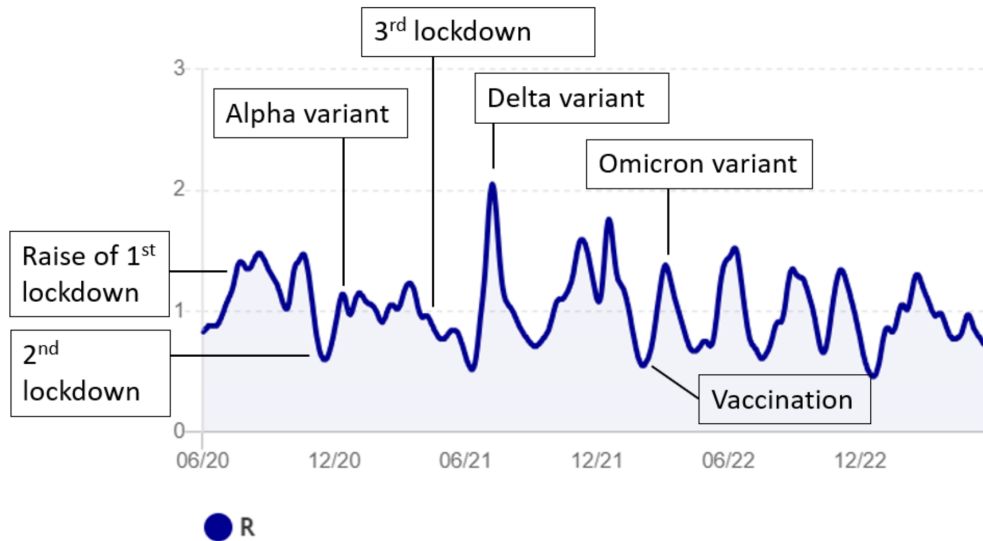


FIG. 1. Evolution of R_{eff} in France during the COVID-19 pandemic between June 2020 and June 2023. R_{eff} corresponds to the effective reproduction number of the virus, that is, the average number of people to which the virus is transmitted by a sick individual. If $R_{\text{eff}} > 1$, then the epidemic grows, and it decreases if $R_{\text{eff}} < 1$. We see that there are very significant variations of R_{eff} which range from 0.6 to 2. We marked on the figure some peaks and valleys that have clearly identified origins (data from “Santé Publique France,” by Guillaume Rozier [10].)

by the model itself, but ideally obtained from epidemic data [1,11]. However, given the amplitude and timescale of these variations, and in spite of the large amounts of data used, exploiting these data involves a lot of guesswork and lead to predictions [12,13] which could be inaccurate, especially on long timescales.

To overcome these difficulties, one needs to introduce models for which the *extrinsic* parameters have no time dependence (at least on the timescale of the epidemic), and which can therefore be fitted in a reliable way on field data. However, all time-dependent parameters, and in particular the ones modeling social interactions, should be *intrinsic*, in the sense that their dynamics should be predicted by the model. This naturally calls for a game theoretical approach (for a review, see Ref. [14]). Here we will follow an approach known as mean-field-game theory.

Introduced by Lasry and Lions almost two decades ago [15–17] and independently by Huang, Malhamé and Caines [18], mean-field games (MFG) focus on the derivation of a Nash equilibrium within a population containing a large number of individuals. Readers may refer to Refs. [19–21] for a complete mathematical description, and to Refs. [22,23] for an introduction aimed at physicists. Applications of MFG include finance [24], economics [25], crowd modeling [26], and opinion dynamics [27], among many others.

The introduction of MFG models to describe epidemics dynamics has been first used a decade ago by Reluga *et al.* [28] about social distancing. Mean-field games have been then used to describe vaccination rates, which appears to be an extrinsic parameter with a dynamics mainly influenced by individuals choices. Pioneers on this matter are Laguzet *et al.* [29] (see also Refs. [29–31]). Recently, a similar approach has been proposed by Elie *et al.* in Ref. [32] to study the impact of individual decisions regarding distancing and isolation, that is, to study human impact on the dynamics of the epidemic (see Refs. [33,34] for a mathematical perspective). An extensive

review of recent progresses in this new field can be found in Ref. [35].

The significant advances made in Ref. [32] establish how the mean-field-game concepts can be implemented to describe the dynamics of social distancing in a simple epidemic model. The goal of this paper is to go one step further toward the implementation of MFG in realistic situation by demonstrating that enough degree of complexity can be introduced within a MFG framework to address questions of practical importance for public institutions, in the context of what is referred to, in the literature, as the nonpharmaceutical interventions (NPI) strategies.

To achieve this goal, this paper is divided in two rather distinct parts. In the first part, Secs. II and III, we introduce at a rather general level the class of models we are interested in, describe the corresponding mathematical framework, and derive the associated dynamical equations. More specifically, Sec. II introduces the SIR model with a social structure on which we base our discussion and Sec. III implements the corresponding MFG paradigm, that is, presents the individual optimization scheme and its consequences at the society scale and formulates the corresponding Nash equilibrium. The central results of this part are Eqs. (2.11) and (2.12) and Eqs. (3.14)–(3.16), and its main content is summarized in the header of Sec. IV, so that readers less interested in the mathematical formalism can go directly to this section.

We then turn, in Secs. IV and V, to the second part of the paper, where we illustrate on a particular example the kind of problematic that can be addressed, and the kind of questions that can be asked, within our formalism. We stress that our goal here is not to analyze a specific epidemics in a specific geographic location, as, on the one hand, the idiosyncrasies of any specific real case would obscure our main message, and since, on the other hand, the specification of the parameters of our model based on real data is clearly beyond the scope of this work. Rather, we will consider a particular

implementation/set of parameters which can be considered as rather typical (we will argue why). In Sec. IV we will discuss, on that example, how the Nash equilibrium differ from, on the one hand, a “business as usual” approach where the agents do not modify their behavior during the epidemics, and, on the other hand, a “societal optima” where each individual is assumed to follow a completely altruistic behavior, focusing in particular on how these different scenario may affect in a rather different way the different age classes. We shall also address in that section the effectiveness of possible lockdowns, and the risk they represent. In Sec. V, we then broaden the discussion and consider the various strategies that public institutions can put in place to mitigate an epidemics through nonpharmaceutical interventions and show in particular the existence of a first-order phase transition as some parameters, such as the duration of the epidemics or the risk due to an infection, are varied. Finally, concluding remarks are assembled in Sec. VI. Some mathematical and numerical details, as well as a more general exploration of the parameter space of our model, are gathered in the Appendix.

II. SOCIAL-STRUCTURE MODELING OF THE EPIDEMICS DYNAMICS

In this section, we introduce and analyze in detail the dynamics of the SIR model with social structure which forms the basis of this work. We start by reviewing briefly the plain-vanilla SIR model.

A. SIR model

Since the early 20th Century, many models have been proposed to model epidemic dynamics, one of the simplest being the susceptible-infected-recovered (SIR) compartment model [36] and its variations [37]. Recently, this model has been refined to take into account the structure of social contacts [38,39], as well as spatial or geographic aspects of the dynamics [40,41].

The SIR model is defined as follows. Individuals can be in three possible states $x = s, i, \text{ or } r$, with $s = \text{“susceptible,”}$ $i = \text{“infected,”}$ and $r = \text{“recovered.”}$ Starting from some initial configuration at $t = 0$, one then assumes that the evolution of the system is Markovian. Between times t and $t + dt$, individuals can switch from one state to another with a certain probability, which depends on their contact rate with the rest of the population and of the status of people they meet. In a population composed of N_{tot} individuals, the probability for an individual k to have contact with another individual l during the interval $[t, t + dt[$ is $\frac{1}{N_{\text{tot}}} \chi(t) dt$, with $\chi(t)$ a (possibly time-dependent) given parameter corresponding to the total contact rate of the individual k . We make the assumption that all individuals can be met by k with equal probability (in other words, the population considered from the point of view of k is homogeneous). If individual l is infected and k susceptible, then there is a probability ρ that the disease be transmitted from l to k upon contact. Last, infected individuals have a probability ξdt to recover from their illness during the interval $[t, t + dt[$, after which they are immune to the disease.

Noting $S(t)$, $I(t)$, and $R(t)$, respectively, the relative proportion of susceptible, infected, and recovered individuals

at time t [thus $S(t) + I(t) + R(t) = 1$], the evolution of the epidemic is governed by the system of equations [36]

$$\begin{aligned}\dot{S} &= -\rho\chi(t)S(t)I(t), \\ \dot{I} &= \rho\chi(t)S(t)I(t) - \xi I(t), \\ \dot{R} &= \xi I(t).\end{aligned}\tag{2.1}$$

This system of equations is almost a century old [36]; we derive it for completeness in Appendix A to prepare for the slightly more involved situation that we are going to consider in this paper. Let us highlight here the two main underlying hypotheses of the derivation of Eq. (2.1): (i) the total contact rate of individual k , $\chi(t)$, is independent on the individual k ; and (ii) N_{tot} is large enough to consider the states of two randomly chosen individuals k and l as independent. We shall keep both these hypotheses to derive dynamical equations for our model introduced in Sec. II B; while hypothesis (ii) is rather harmless in practice where N_{tot} is large, hypothesis (i) is an important assumption which can be discussed in practice.

Figure 2 summarizes the process that drives an individual from state s to i to r . The system of equations (2.1) only involves average quantities S , I , and R , which are determined as solutions of the system. Furthermore, it is characterized by two extrinsic parameters, the recovery rate ξ and the product of the contact rate $\chi(t)$ by the probability ρ of transmitting the disease, which must be obtained from observation data [13]. For virus epidemics like COVID-19, with a very fast dynamics, this is a challenging task. Major efforts have been invested by the epidemiologist community to extract these parameters, or their counterpart in more complex models, from the actual data observed on the field. While ξ is mainly fixed by biological considerations, and considered constant in time in the present model, the contact rate $\chi(t)$, however, depends a lot on the agent’s behavior, that is, how social they are (or are allowed to be); that behavior may vary strongly with time, and in a way that may depend on the dynamics of the epidemic itself. A consequence of this retroaction is that it is essentially impossible to fit the time dependence of $\chi(t)$ on past data. In models used to advise public policies, this time dependence is thus either simply ignored, or involves a lot of guesswork [12], leading to predictions that can be trusted only for a rather short amount of time [13] (see, nevertheless, Refs. [1,42]).

What we discussed above is the simplest version of the SIR model. A number of variations can be found in the literature, that aim to gain in precision. The most common ones are the SIRD model (D for deceased [43]), SIRV (V for vaccination [44]), MSIR (M for maternally derived immunity [37]), SIRC (C for carrier but asymptomatic [45]), or SEIR models (E for exposed class [46]), to name a few—see Ref. [37] for a more detailed literature on the subject of compartmental models. However, there are two essential limitations of these models: they assume that the population is entirely uniform, and they take parameters such as the contact rates as extrinsic.

Let us expand slightly on these two issues. The first limitation is that these models assume a homogeneous population: all individuals are expected to act in the same way, have the same contact rate with all other individuals (in a given compartment), and behave similarly with respect to the epidemic. Of course, this is not true, and social heterogeneity has an



FIG. 2. Illustration of the Markov process for the classic SIR model with the transition rates to move from one state to another between time t and $t + dt$. An individual susceptible at t has a probability $\rho\chi(t)I(t)dt$ to become infected. If this individual is already infected at t , then she will have a constant probability ξdt to recover from the disease.

important impact on epidemics modeling. As an example, epidemics inside schools have a different and faster dynamics than can be expected from the SIR model, because children have a lot of contacts with each other and they live together during a long part of the day. To address this issue, SIR models with a structure of social contacts were proposed in Refs. [38] and [39] to get a more detailed description of the society at a mesoscopic scale. We will address that limitation by introducing a refined model in Sec. II B. The second limitation of SIR models, already discussed in the introduction, is that the contact rates are extrinsic parameters, fixed at the beginning of the dynamical process. A more realistic approach is to consider that people change their behavior as the epidemic unfolds, so that contact rates should be updated according to the dynamics of the epidemic. We shall circumvent this issue by taking a MFG approach to our model with a social structure in Sec. III, where contact rates will become intrinsic parameters, co-evolving with the epidemic.

B. SIR model with social structure

1. Social structure and contact rates

We now introduce a SIR model with a social structure, in the spirit of Ref. [38]. In this model, rather than taking society as monolithic, we consider a refined description of social contacts. Namely, we introduce three age classes: young, adult and retired, and we assume that individuals have contacts with one another in four different settings: schools, households, community and workplaces; of course a larger number of age classes and settings could easily be implemented. The

structure of the population is illustrated in Fig. 3. We assume the total size of the population, N_{tot} , to be large.

In our model, following Ref. [38], interactions between individuals depend on two factors: the setting $\gamma \in \{\text{school, workplace, community, household}\}$ in which they meet, and their age class $\alpha \in \{\text{young, adult, retired}\}$. We denote by N_{α}^{tot} the total number of individuals in class α . We first consider the simple case of a single setting where interactions only depend on age class, which will be labeled by the Greek letters α or β ; extension to the case of multiple settings is then straightforward.

For two given age classes α and β we define $\mathcal{W}_{\alpha\beta}dt$ as the probability for a pair of individuals $a \in \alpha, b \in \beta$ drawn at random to be in contact during a time interval dt . This means that among all possible $N_{\alpha}^{\text{tot}}N_{\beta}^{\text{tot}}$ pairs, only $\mathcal{W}_{\alpha\beta}N_{\alpha}^{\text{tot}}N_{\beta}^{\text{tot}}dt$ encounters occur during dt . This is illustrated by the graph of Fig. 4; it is similar to Erdős-Renyi graphs, where each potential edge is realized with some probability. In the present case, all potential edges between vertices from one class to the other are realized with some probability that depends on the two classes they connect. A given individual $a \in \alpha$ encounters on average a number $\mathcal{W}_{\alpha\beta}N_{\beta}^{\text{tot}}dt$ of individuals of class β during dt .

A natural assumption, in the spirit of compartmental models, is that behavior of individuals toward different age classes is differentiated, but that a given age class is considered homogeneous from the point of view of an individual. That is, an individual $a \in \alpha$ can decide whether she chooses to encounter members of class β or not, but does not decide which individuals she may encounter in that class. In other words, any individual $a \in \alpha$ willing to meet someone from

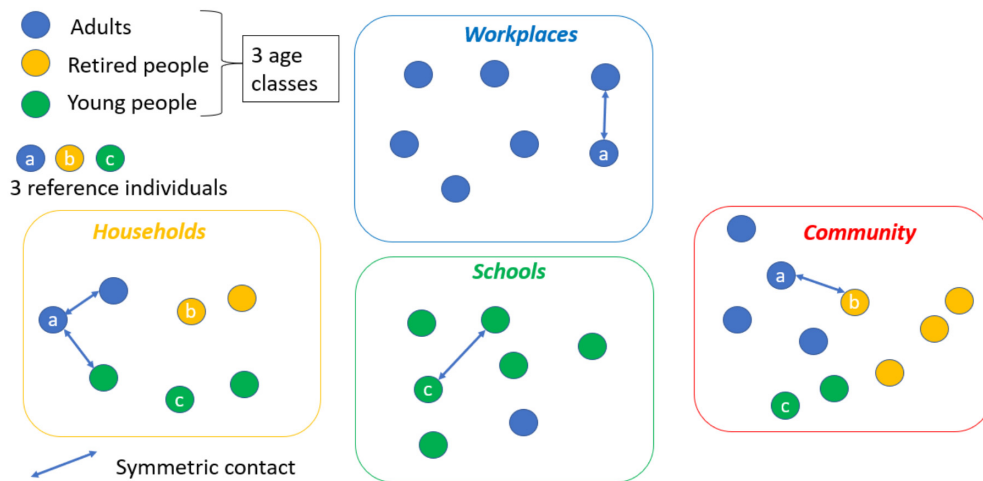


FIG. 3. Graphical illustration of the social structure we implemented. A reference individual (a, b , and c for each age class) will have (symmetric) contacts in each setting, with different type of individuals (more adults at workplaces, more children at school, etc.). The precise structure of interactions is detailed in the following section.

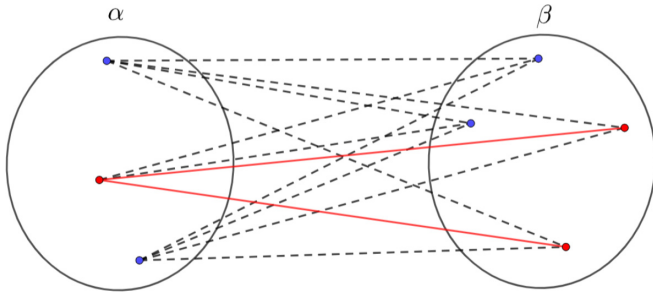


FIG. 4. Graphical illustration of the interactions in our model. Two age classes α and β are represented, here with $N_\alpha^{\text{tot}} = 3$ individuals of age class α and $N_\beta^{\text{tot}} = 4$ of class β . Each vertex is either “active” (in red) if the corresponding individual is willing to have contact with the other class, or “inactive” (in blue). The $N_\alpha^{\text{tot}}N_\beta^{\text{tot}}$ possible contacts are represented in dashed black lines, and effective contacts between pairs of active individuals are red solid lines. Here we have $w_{\alpha\beta}N_\alpha^{\text{tot}} = 1$ active individual of age class α and $w_{\beta\alpha}N_\beta^{\text{tot}} = 2$ active individuals of age class β , which gives $w_{\alpha\beta} = \frac{1}{3}$ and $w_{\beta\alpha} = \frac{1}{2}$. The probability for a randomly chosen pair to be in contact is $\mathcal{W}_{\alpha\beta} = w_{\alpha\beta}w_{\beta\alpha} = \frac{1}{6}$. The average number of contacts with β for an individual $a \in \alpha$ is $\mathcal{W}_{\alpha\beta}N_\beta^{\text{tot}} = \frac{2}{3}$. Similarly, the average number of contacts with α for an individual $b \in \beta$ is $\mathcal{W}_{\beta\alpha}N_\alpha^{\text{tot}} = \frac{1}{2}$. The total number of contacts between the two classes, corresponding to the number of red links in the graph, is given by $N_\beta^{\text{tot}}N_\alpha^{\text{tot}}\mathcal{W}_{\alpha\beta} = 2$.

class β will possibly meet all individuals from class β who themselves are willing to meet individuals from class α . At each time, an individual $a \in \alpha$ can decide whether she is open or close to interactions with class β . Let us denote by $w_{\alpha\beta} \in [0, 1]$ the fraction of individuals $a \in \alpha$ open to meet people from class β . The willingness $w_{\alpha\beta}$ thus indicates the probability of an individual a taken at random in α to be open to contacts with class β . There are $w_{\alpha\beta}N_\alpha^{\text{tot}}$ individuals $a \in \alpha$ willing to meet people with class β , and $w_{\beta\alpha}N_\beta^{\text{tot}}$ individuals $b \in \beta$ willing to meet people from class α . A contact becomes effective (i.e., occurs with probability dt in the interval $[t, t + dt]$) only if both individuals are willing, and therefore among all $N_\alpha^{\text{tot}}N_\beta^{\text{tot}}$ possible links between α and β , only $w_{\alpha\beta}N_\alpha^{\text{tot}} \times w_{\beta\alpha}N_\beta^{\text{tot}}dt$ are realized during dt . As mentioned above, the number of pairs effectively realized can also be expressed as $\mathcal{W}_{\alpha\beta}N_\alpha^{\text{tot}}N_\beta^{\text{tot}}dt$, hence $\mathcal{W}_{\alpha\beta} = w_{\alpha\beta}w_{\beta\alpha}$ (and $\mathcal{W}_{\alpha\beta}$ is a symmetric array, as it should be).

In “normal times,” that is in the absence of epidemic threats, the contact willingness of an individual of class α with class β is a constant $w_{\alpha\beta}^{(0)}$. During an epidemics, however, the agent will adapt her behavior to mitigate the risk of infection, and we assume the contact willingness to take the form

$$w_{\alpha\beta}(t) = n_\alpha(t)w_{\alpha\beta}^{(0)}, \quad (2.2)$$

that is, her initial willingness is modulated by a time-dependent coefficient $n_\alpha(t)$ which measures the effort made by agents in the class α to limit their contacts with others. For simplicity we suppose that this effort is independent of β , but a β dependence can easily be implemented to this model and only slightly changes the equations. We additionally assume that $n_\alpha(t) \in [n_{\alpha,\text{min}}, 1]$, with $n_{\alpha,\text{min}}$ the maximum effort that can be expected from an agent in class α ; the upper bound

TABLE I. Biological parameters and parameters defining the structure of the society. The number of parameters implied by this list is significant, since in particular the array $\mathcal{W}_{\alpha\beta}^{(0)}$ has $3 \times 3 \times 4 = 36$ entries. However, the methodology to get these parameters in any specific implementation is relatively well established (see, e.g., discussion in Appendix B).

Parameter	Definition
ρ	Probability of transmission per contact
μ	Proportion of asymptomatic individuals in the population
ξ	Recovery rate
N_α^{tot}	Number of individuals of age class α
$\mathcal{W}_{\alpha\beta}^{(0)} = w_{\alpha\beta}^{(0)}w_{\beta\alpha}^{(0)}$	Willingness of contacts between two age classes α and β (symmetric in $\alpha \leftrightarrow \beta$)

1 corresponds to the natural assumption that the epidemic situation can only reduce the initial willingness.

2. Asymptomatic individuals

Interactions between individuals may vary with time, but also differ between different age classes and in different settings. As a result, the dynamics of the epidemic will be different in each subcategory. This turns out to be particularly relevant for susceptible agents, and we will go back to this in more details in the next subsection. But the issue could be raised also for infected individuals whose behavior may range from a completely egoistic one, in which they stop limiting their contacts since they are not worried any more about being infected, to being completely altruistic and isolate themselves from the rest of population. To make things more concrete, we assume this latter option, but also assume that a fraction μ of the population is asymptomatic (they do not know if they are infected or not) and hence behave as susceptible, while the other fraction $1 - \mu$ is symptomatic and stay home to protect others. This additional status (symptomatic or asymptomatic) is random in the population and is fixed at the beginning of the epidemic. Therefore, the epidemic is only spread by individuals who are both asymptomatic and infected. They represent a fraction $\mu I(t)$ of the population. We summarize our model in Fig. 5.

The parameters defining our SIR model with social structure can thus be divided in two groups. On the one hand, we have three “biological” parameters: the probability ρ of transmission of the virus per effective contact between a susceptible and an infected individual, the fraction μ of the infected population which is asymptomatic, and the recovery rate ξ . On the other hand, the social structure is defined by the number of individuals N_α^{tot} in the age classe α and by the coefficients $\mathcal{W}_{\alpha\beta}^{(0)} \equiv w_{\alpha\beta}^{(0)}w_{\beta\alpha}^{(0)}$ determining the structure of our society, i.e., the contact rates in the absence of the epidemics. Table I summarizes this information.

For a given epidemic in a given geographic location, determining the parameters of Table I follows *a priori* a well-defined, though not necessarily straightforward, path, both for the “biologic parameters” (ρ, μ, ξ) typically encountered in traditional SIR-like models [47], but also for the ones associated with the social structure [39]. Much less straightforward

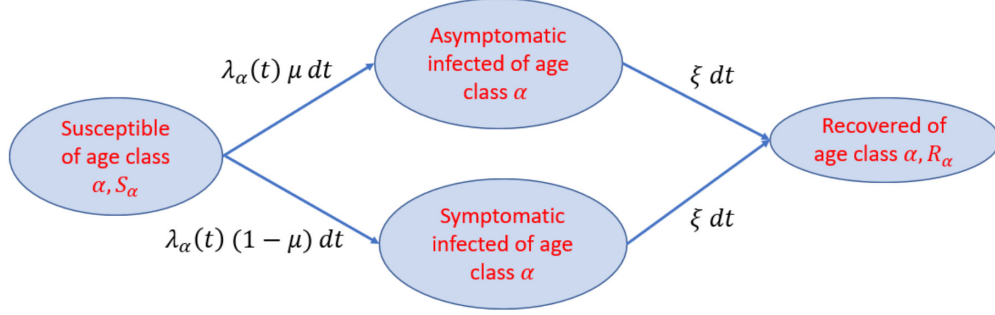


FIG. 5. Graphical illustration of the particular SIR model we use. An individual infected at time t has a probability μ to be asymptomatic and $1 - \mu$ to be symptomatic. The force of infection λ_α is derived in Sec. II B 3 and drives the probability of infection $\lambda_\alpha dt$. Then, all individuals have a constant recovery rate ξ to recover from the disease.

is the determination of the time dependence of the “effort parameters” $n_\alpha(t)$ introduced in Eq. (2.2). For the rest of Sec. II B, we assume these $n_\alpha(t)$ known, and we will discuss how their dynamics can be analyzed in Sec. III.

3. Time evolution equations

We now derive the time evolution equations of the epidemic quantities for this model. The fraction of susceptible (respectively, infected, recovered) individuals in class α is S_α (respectively, I_α , R_α), with $S_\alpha + I_\alpha + R_\alpha = 1$. To establish the mean-field equations, we single out a reference individual $a \in \alpha$ who is susceptible at time t and has status $x_a(t) = s$, i or r at subsequent times. We furthermore here lift the hypothesis that all individuals of a given age class behave in exactly the same way, and we assume that the reference individual has her own time-dependent strategy $n_a(t)$ and willingness $w_{a\beta}(t) = n_a(t)w_{\alpha\beta}^{(0)}$, with, however, the understanding that n_α is the average over susceptible individuals of n_a , which we express as

$$n_\alpha = \frac{1}{S_\alpha N_{\text{tot}}} \sum_a n_a \delta_{x_a, s}. \quad (2.3)$$

Let $b \in \beta$ be an individual of class β , whose willingness to meet class α is $w_{b\alpha}(t) = n_b(t)w_{\beta\alpha}^{(0)}$. For a to be contaminated by b during $[t, t + dt]$, b must be infected and asymptomatic, and a and b must meet; contamination then occurs with probability ρ . Distinguishing within the $i =$ “infected” status between $i_a =$ “asymptomatic infected” and $i_s =$ “symptomatic infected”, the probability that a become infected by b during $[t, t + dt]$ is therefore

$$P_{ab}(t)dt = \rho n_a(t) n_b(t) \mathcal{W}_{\alpha\beta}^{(0)} \delta_{x_b(t), i_a} dt, \quad (2.4)$$

where we used the fact that $w_{\alpha\beta}^{(0)} w_{\beta\alpha}^{(0)} = \mathcal{W}_{\alpha\beta}^{(0)}$ (see Table I). Taking the sum over all $b \in \beta$ and all age classes β we get the total probability that an individual a susceptible at time t is infected between t and $t + dt$

$$P_a(t)dt := \mathcal{P}[x_a(t + dt) = i | x_a(t) = s] = \sum_\beta \sum_{b \in \beta} P_{ab}(t)dt, \quad (2.5)$$

with $\mathcal{P}[e]$ the probability of the event e .

We then follow the same reasoning as in the SIR case [see Eq. (A3)]. Averaging over all individuals $a \in \alpha$ and over realizations of the Markov process, and summing over age

classes β , we obtain

$$\frac{dS_\alpha(t)}{dt} = -\frac{1}{N_\alpha^{\text{tot}}} \sum_{a=1}^{N_\alpha^{\text{tot}}} \delta_{x_a(t), s} P_a(t) \quad (2.6)$$

$$= -\rho \sum_\beta \mathcal{W}_{\alpha\beta}^{(0)} \left(\frac{1}{N_\alpha^{\text{tot}}} \sum_{a=1}^{N_\alpha^{\text{tot}}} n_a(t) \delta_{x_a(t), s} \right) \times \left(\sum_{b=1}^{N_\beta^{\text{tot}}} n_b(t) \mu \delta_{x_b(t), i} \right) \quad (2.7)$$

$$= -\rho \sum_\beta \mathcal{W}_{\alpha\beta}^{(0)} (S_\alpha n_\alpha) (\mu N_\beta^{\text{tot}} I_\beta n_\beta). \quad (2.8)$$

To get this last expression, Eq. (2.3) was used, together with the assumption that asymptomatic infected individuals responsible for contamination behave on average in the same way as susceptible individuals, so that we have also for all age classes

$$n_\beta(t) = \frac{1}{\mu I_\beta N_\beta^{\text{tot}}} \sum_{b \in \beta} n_b(t) \delta_{x_b(t), i_a}. \quad (2.9)$$

Equation (2.8) can then be written as

$$\frac{dS_\alpha}{dt} = -\lambda_\alpha(t) S_\alpha(t), \quad (2.10)$$

where, performing the straightforward generalization to include different settings γ ,

$$\lambda_\alpha(t) \equiv \mu \rho \sum_{\beta=1}^{n_{\text{cl}}} N_\beta^{\text{tot}} \sum_{\gamma=1}^{n_{\text{set}}} n_\alpha^\gamma(t) n_\beta^\gamma(t) \mathcal{W}_{\alpha\beta}^{\gamma(0)} I_\beta(t), \quad (2.11)$$

with n_{cl} and n_{set} , respectively, the number of classes and settings in the social structure. Equation (2.10) is the analog of the SIR Eq. (A5) but in the case of a population with social structure. The two other equations analogous to the system (2.1) are derived in the same way. The system of coupled differential equations for the SIR model with social structure finally reads

$$\begin{aligned} \dot{S}_\alpha &= -\lambda_\alpha(t) S_\alpha(t), \\ \dot{I}_\alpha &= \lambda_\alpha(t) S_\alpha(t) - \xi I_\alpha(t), \\ \dot{R}_\alpha &= \xi I_\alpha(t). \end{aligned} \quad (2.12)$$

These equations are the main equations of our SIR model with a social structure. Once the “interaction strategies” $n_\alpha^\gamma(\cdot)$ are fixed for each age class α and each setting γ , one can solve Eq. (2.12) and obtain the dynamic of the relative proportion of susceptible, infected and recovered in each class. However, for rational agents interaction strategies should depend on the evolution of the epidemic. To address this interplay, we need the machinery of mean-field games, which we now introduce.

III. MEAN-FIELD-GAME APPROACH: INDIVIDUAL OPTIMIZATION

To address the dynamics of the willingness $w_{\alpha\beta}^\gamma(t)$ requires a game theoretical approach, which implies a control parameter that the agents can choose a will, and a cost function that they try to optimize. In our model, the control parameter defining the “strategy” of a given agent a is quite naturally the function $n_a^\gamma(t)$, which reflects her desire to have contact with someone in each setting γ .

Turning now to the cost function, consider a fixed individual $a \in \alpha$. If a has no symptoms at time t , then she estimates the cost she will incur because of the the epidemic as the sum of two terms: one due to the cost of infection if it happens, and one associated with the cost of efforts to avoid the infection. If a becomes infected at some time $\tau > t$, then the total cost paid between t and the end of the optimization process at T is

$$C_a(n_a^\gamma(\cdot), \{n_\beta^\gamma(\cdot)\}, t, \tau) \equiv \mathcal{I}_\alpha(I(\tau))\mathbb{1}_{\tau < T} + \int_t^{\min(\tau, T)} f_\alpha(n_a^\gamma(t')) dt'. \quad (3.1)$$

This cost is an explicit function of τ the time of infection, and of the strategies $n_a^\gamma(\cdot)$ of a in each setting and at each time between t and $\min(\tau, T)$. It also depends implicitly, through the (average) proportion of infected at time τ , $I(\tau) \equiv \frac{1}{N_{\text{tot}}} \sum_\alpha N_\alpha^{\text{tot}} I_\alpha(\tau)$, on all the strategies $\{n_\beta^\gamma(\cdot)\}$ for all age classes β (including α) and settings γ in the same time interval. The first term in Eq. (3.1) is the total cost of infection $\mathcal{I}_\alpha(I(\tau))$ paid by the agent once she is infected. This cost can include financial cost, as the loss of income incurred by not working, the costs of medical treatment or hospitalization, but also moral and psychological costs associated with the pain of going through the illness, permanent health damage, or death. We assume that this cost of infection depends on the age class and on the (average) proportion $I(\tau)$ of infected, reflecting the pressure on the sanitary system. In the second term, $f_\alpha(n_a^\gamma(s))$ measures the cost (both psychological and financial) associated with the limitation of social contacts (incurred, for instance, by the inability of doing business); this cost can be different according to the age class of the individual, and depends on the behavior of the individual only. At each time s between t and τ (the time of infection) or T (if the agent is never infected) the agent will pay a cost $f_\alpha(n_a^\gamma(s))ds$; for $s > \tau$ we have $f_\alpha = 0$, as the individual is either infected (in which case the social cost is included in the term \mathcal{I}_α) or recovered (as there is no possible new infection in our model).

We now derive the optimization made by the agents, following in the spirit of Turinici *et al.* in Ref. [32].

A. Calculation of the expected cost \mathfrak{C}_a

We assume here $\mu \ll 1$. As shown in Appendix C, considering a finite μ makes notations slightly heavier without changing qualitatively the dynamics of the epidemics. Therefore in the rest of the paper we shall restrict ourselves to the regime $\mu \ll 1$.

In that case, almost all infected individuals are symptomatic, and thus individuals with no symptoms can estimate their future cost neglecting the probability that they might be infected. Note however that contamination still occurs via the few infected asymptomatic individuals.

Consider a fixed individual $a \in \alpha$, who incurs the cost Eq. (3.1) as a function of the time of infection τ and of her strategy (for all setups γ and all times t) $n_a^\gamma(t)$. From the perspective of agent a at time t , and since the epidemic propagation is a stochastic process, the time of infection τ is a random variable that changes from one realization of the epidemic to the other. We denote

$$\tilde{P}_a(\tau) d\tau = \mathcal{P}[x_a(\tau + d\tau) = i \& x_a(\tau) = s] \quad (3.2)$$

as the probability that the individual a is infected during the time interval $[\tau, \tau + d\tau[$. Note this probability is a *functional* of $n_a^\gamma(t')$, $t' \in [t, \tau]$, and of the strategies $\{n_\beta^\gamma(t')\}$, $t' \in [t, \tau]$ since these latter will determine the $I_\beta(\tau)$, and thus the probability that an individual met at time τ is or not infected. \tilde{P}_a is also a function of t since the agent has acquired information about whether or not she has been infected in the interval $[0, t]$. The cost in Eq. (3.1) is thus also a stochastic variable, and at each time t , a rational agent should choose her future strategies in each setting $n_a^\gamma(t')$, $t' > t$, as the ones that minimize the *average* value of C_a over random realizations,

$$\mathfrak{C}_a(n_a^\gamma(\cdot), \{n_\beta^\gamma(\cdot)\}, t) \equiv \int_t^\infty d\tau \tilde{P}_a(\tau) C_a(n_a^\gamma(\cdot), \{n_\beta^\gamma(\cdot)\}, t, \tau), \quad (3.3)$$

where formally we understand $\tau > T$ as an absence of infection (so that we can normalize $\int_t^\infty \tilde{P}_a(\tau) d\tau = 1$, and $C_a(n_a^\gamma(\cdot), \{n_\beta^\gamma(\cdot)\}, t, \tau > T) = \int_t^T f_\alpha(n_a^\gamma(t')) dt'$).

We now need to evaluate the probability $\tilde{P}_a(\tau)$ for an agent a who is assumed to follow a specific strategy $n_a^\gamma(\cdot)$. Let $\phi_a(\tau)$ be the corresponding cumulative probability, that is, the probability for a to be infected before time τ (the probability that a is susceptible at some arbitrary time t is thus $\mathcal{P}[x_a(t) = s_\alpha] = 1 - \phi_a(t)$). The probability that the infection time for a is between τ and $\tau + d\tau$ is

$$\phi'_a(\tau) d\tau = \tilde{P}_a(\tau) d\tau = \mathcal{P}[x_a(\tau + d\tau) = i_\alpha | x_a(\tau) = s_\alpha] \times \mathcal{P}[x_a(\tau) = s_\alpha], \quad (3.4)$$

where the first term of the right-hand side is obtained from Eqs. (2.5) and (2.9), giving

$$\mathcal{P}[x_a(\tau + d\tau) = i_\alpha | x_a(\tau) = s_\alpha] = \lambda_a(\tau) d\tau, \quad (3.5)$$

with

$$\lambda_a(t) \equiv \mu \rho \sum_{\beta=1}^{n_{\text{cl}}} N_\beta^{\text{tot}} \sum_{\gamma=1}^{n_{\text{set}}} n_a^\gamma(t) n_\beta^\gamma(t) \mathcal{W}_{\alpha\beta}^{\gamma(0)} I_\beta(t) \quad (3.6)$$

as the force of infection seen by individual a . This individual force of infection differs from the collective one Eq. (2.11)

only by the replacement of the collective behavior n_α^γ by the individual strategy n_a^γ (for all settings γ). Equation (3.4) thus leads to $\phi_a'(\tau) = \lambda_a(\tau)(1 - \phi_a(\tau))$, which together with $\phi_a(t) = 0$ gives

$$\phi_a(\tau) = 1 - \exp\left(-\int_t^\tau \lambda_a(s) ds\right). \quad (3.7)$$

The average cost (3.3) then reads

$$\begin{aligned} \mathfrak{C}_a(n_a^\gamma(\cdot), \{n_\beta^\gamma(\cdot)\}, t) &= \int_t^T d\tau \tilde{P}_a(\tau) \mathcal{I}_\alpha(I(\tau)) \\ &\quad + \int_t^\infty d\tau \tilde{P}_a(\tau) \int_t^{\min(\tau, T)} ds f_\alpha(n_a^\gamma(s)) \\ &= \int_t^T dt' \tilde{P}_a(t') \mathcal{I}_\alpha(I(t')) \\ &\quad + \int_t^T dt' f_\alpha(n_a^\gamma(t')) \int_{t'}^\infty d\tau \tilde{P}_a(\tau). \end{aligned} \quad (3.8)$$

We then use the fact that $\phi_a'(\tau) = \tilde{P}_a(\tau) = \lambda_a(\tau)(1 - \phi_a(\tau))$ to get

$$\begin{aligned} \mathfrak{C}_a(n_a^\gamma(\cdot), \{n_\beta^\gamma(\cdot)\}, t) \\ = \int_t^T [\lambda_a(s) \mathcal{I}_\alpha(I(s)) + f_\alpha(n_a^\gamma(s))] (1 - \phi_a(s)) ds. \end{aligned} \quad (3.9)$$

In the following, we will often use $\mathfrak{C}_a(n_a^\gamma, t)$ for simplicity, but the cost still depends implicitly on all the $n_\beta^\gamma(\cdot)$.

B. Hamilton-Jacobi-Bellman equations

The expected cost at time t for agent a is a function of her own strategy n_a and of the epidemic functions $S(\cdot), I(\cdot), R(\cdot)$. The next step is to solve the optimization problem, that is, find the optimal strategy n_a^* for a given epidemic $S(\cdot), I(\cdot), R(\cdot)$. Following a standard approach in this context [20], we introduce the *value function*

$$U_a(t) = \begin{cases} \min_{n_a^\gamma(\cdot)} \mathfrak{C}_a(n_a^\gamma(\cdot), t), & a \text{ susceptible at } t, \\ 0, & a \text{ infected at } t. \end{cases} \quad (3.10)$$

This corresponds to the minimal cost that an agent has to pay between t and the end of the game (averaged over random realizations of the game, and assuming that all other players follow some given strategies n_β^γ). Note that in Eq. (3.1) we assumed that the total cost of infection is paid right after infection, so that individuals do not incur any additional cost at later times. The Markov process of the game is described by the following equations, illustrated in Fig. 5:

$$\begin{aligned} \tilde{P}_a(x_a(t+dt) = i_\alpha | x_a(t) = s_\alpha) &= \lambda_a(t) dt, \\ \tilde{P}_a(x_a(t+dt) = s_\alpha | x_a(t) = s_\alpha) &= 1 - \lambda_a(t) dt, \\ \tilde{P}_a(x_a(t+dt) = r_\alpha | x_a(t) = i_\alpha) &= \xi dt. \end{aligned} \quad (3.11)$$

We use a standard Bellman argument to find the evolution of U_a : the lowest possible cost at time t is given by adding two quantities: the lowest possible cost at time $t+dt$, and the cost incurred in the interval $[t, t+dt[$ associated with the optimal

strategy at t . Assuming a status $x_a(t) = s_\alpha$ at time t , this can be expressed as

$$U_a(t) = \min_{n_a^\gamma(t)} \mathbb{E}_{x_a(t+dt)} [U_a(t+dt) + c_a(t)], \quad (3.12)$$

with $c_a(t)$ the cost paid in the interval $[t, t+dt[$. At time $t+dt$, the agent either is still susceptible, or becomes infected. If $x_a(t+dt) = s_\alpha$, then the only cost at t is $c_a(t) = f_\alpha(n_a^\gamma(t))dt$, whereas if $x_a(t+dt) = i_\alpha$ then a has to bear the costs due to infection, and thus $c_a(t) = \mathcal{I}_\alpha(I(t))$. Following Eq. (3.10), if a is susceptible at $t+dt$, then the quantity $U_a(t+dt)$ involves the average cost $\mathfrak{C}_a(n_a^\gamma(\cdot), t+dt)$, which is an average over all random realizations of the epidemic at times $t' > t+dt$; if a is infected at $t+dt$, then $U_a(t+dt) = 0$. The expectation value in Eq. (3.12) is therefore taken over random realizations of the status $x_a(t+dt)$.

Writing explicitly the expectation in Eq. (3.12) and using the probabilities given by Eq. (3.11) we get

$$\begin{aligned} U_a(t) = \min_{n_a^\gamma(t)} [\mathcal{I}_\alpha(I(t)) \lambda_a(t) dt + (1 - \lambda_a(t) dt) (U_a(t+dt) \\ + f_\alpha(n_a^\gamma(t)) dt)]. \end{aligned} \quad (3.13)$$

At first order in dt , this gives the Hamilton-Jacobi-Bellman (HJB) equation of our mean-field game

$$-\frac{dU_a(t)}{dt} = \min_{n_a^\gamma(t)} [\lambda_a(t) (\mathcal{I}_\alpha(I(t)) - U_a(t)) + f_\alpha(n_a^\gamma(t))], \quad (3.14)$$

and the optimal strategy $n_a^{\gamma*}(t)$ at time t is given by

$$n_a^{\gamma*}(t) = \operatorname{argmin}_{n_a^\gamma(t)} [\lambda_a(t) (\mathcal{I}_\alpha(I(t)) - U_a(t)) + f_\alpha(n_a^\gamma(t))], \quad (3.15)$$

where the optimization is now performed for a given, *fixed*, time. By taking a particular form for f_α , one can compute $n_a^{\gamma*}(t)$ by setting to zero the derivative of the right-hand side with respect to n . Thus, for a given epidemic, we can obtain the optimal individual behavior backward in time by solving HJB Eq. (3.14). More details will be given in Sec. IV D.

C. Nash equilibrium

The outcome of Secs. II B and III B can now be summarized as follows. Assuming the global (or average) strategies $n_\alpha^\gamma(\cdot)$ known, the time evolution of the epidemics variables $S_\alpha(t), I_\alpha(t), R_\alpha(t)$ are derived from Eqs. (2.11) and (2.12). From the knowledge of these epidemic variables, an individual a of age class α can perform an individual optimization leading to the optimal strategy $n_a^{\gamma*}(t)$ given by Eq. (3.15).

A (symmetric) Nash equilibrium corresponds to the situation in which this individual optimization actually coincides with the global strategy of class α , which leads to the self-consistent equation

$$n_a^{\gamma*}(\cdot) = n_\alpha^\gamma(\cdot) \quad (3.16)$$

for all age classes α and all settings γ . Under this self-consistent condition an agent can indeed assume that the other individuals will follow the strategies $n_\alpha^\gamma(\cdot)$ as this will indeed correspond for them to an individual optimum, as it does for her. ‘‘Solving’’ our mean-field game will therefore amount to

solve the (forward) rate equations Eqs. (2.11) and (2.12) together with the (backward) HJB equation Eq. (3.14) and with the self-consistent (Nash equilibrium) condition Eq. (3.16).

IV. EPIDEMICS DYNAMICS

In Secs. II and III we described the formalism of our MFG theory of SIR-models with social structure; in the present section we implement the corresponding equations, discuss the resulting epidemics dynamics and analyze the different types of optimal strategies. We shall choose a particular setting to best illustrate what kind of problems can be addressed and what kind of questions can be asked within this framework. Once again, we stress that we do not aim at describing a specific epidemic breakout in a given geographic area with parameters extracted from real data: this would clearly be beyond the reach of this work. Our choice in the present section is to consider a rather “typical” configuration and discuss the kind of information that could be extracted from our model, and how it could be used by public institutions; a more thorough exploration of the model’s parameter space will be performed in Appendix G. We start by giving a brief summary of our MFG formalism in Sec. IV A. In Sec. IV B we introduce the specific form of the cost function and the choice of parameters that we will discuss, and in Sec. IV C we introduce different scenarios, corresponding to different choices or constraints on the contact willingness, and summarize the results obtained from solving the equations. These different scenarios are defined in more detail in the subsequent subsections: unconstrained Nash equilibrium in Sec. IV D, Nash equilibrium with constraints (e.g., partial lockdown imposed by a centralized authority) in Sec. IV E, societal optimum (where a global planner controls perfectly the behavior of each agent to minimize the total costs borne by the society) in Sec. IV F. Finally, in Sec. IV G 1 we compare the different scenarios.

A. Summary of Secs. II and III

Before we dive into a detailed analysis of the kind of behavior that may emerge within our MFG model, let us summarize briefly the content of the two previous sections. We have first introduced in Sec. II B a SIR model with social structure in which we distinguish three age classes $\alpha \in \{\text{young, adult, retired}\}$ and different settings $\gamma \in \{\text{schools, household, communities, workplace}\}$. In addition to the time-dependent variables $n_\alpha^\gamma(t) \in [n_{\min}^\gamma, 1]$ corresponding to the effort made by individuals in the setting γ to avoid infection, the model is characterized by three “biological parameters” (the probability ρ of transmission of the disease per contact, the proportion μ of asymptomatic individuals in the infected population, and the recover rate ξ), and a set of “social-structure parameters” (the number of individuals N_α^{tot} in each age class, and the array $\mathcal{W}_{\alpha\beta}^{\gamma(0)}$ specifying the contact rate of the agents in the absence of epidemics); cf Table I.

One remark is in order here. The N_α^{tot} and (the inverse of) $\mathcal{W}_{\alpha\beta}^{\gamma(0)}$ are *extensive* quantities: as $N_{\text{tot}} \rightarrow \infty$, so does the N_α^{tot} , and the $\mathcal{W}_{\alpha\beta}^{\gamma(0)}$ have to go to zero to maintain a finite rate of infection for a given individual. While the formal developments of Secs. II and III were better performed using

theses variables, we shall from now on use related *intensive* parameters, which are well-defined in the limit $N_{\text{tot}} \rightarrow \infty$ and easier to relate to observable data. We thus introduce $\mathcal{N}_\alpha = N_\alpha^{\text{tot}}/N_{\text{tot}}$, the proportion of agents in age class α , and the array

$$\mathcal{M}_{\alpha\beta}^{\gamma(0)} := \mathcal{W}_{\alpha\beta}^{\gamma(0)} N_\beta^{\text{tot}}, \quad (4.1)$$

which corresponds to the average number of contacts with β for an individual $a \in \alpha$. The requirement that $\mathcal{W}_{\alpha\beta}^{\gamma(0)}$ is a symmetric matrix implies the constraint $\mathcal{N}_\alpha \mathcal{M}_{\alpha\beta}^{\gamma(0)} = \mathcal{N}_\beta \mathcal{M}_{\beta\alpha}^{\gamma(0)}$, for all age class pairs (α, β) and all settings γ .

In terms of these parameters, the dynamics of the epidemic variables given by Eqs. (2.11) and (2.12) takes the form

$$\begin{aligned} \dot{S}_\alpha &= -\lambda_\alpha(t) S_\alpha(t), \\ \dot{I}_\alpha &= \lambda_\alpha(t) S_\alpha(t) - \xi I_\alpha(t), \\ \dot{R}_\alpha &= \xi I_\alpha(t). \end{aligned} \quad (4.2)$$

$$\lambda_\alpha(t) \equiv \mu \rho \sum_{\beta=1}^{n_{\text{cl}}} \sum_{\gamma=1}^{n_{\text{set}}} n_\alpha^\gamma(t) n_\beta^\gamma(t) \mathcal{M}_{\alpha\beta}^{\gamma(0)} I_\beta(t). \quad (4.3)$$

Within our mean-field-game approach, the dynamics of the variables $n_\alpha^\gamma(\cdot)$ is determined by an optimization of the intertemporal cost Eq. (3.1) which is characterized, for each age class α , by two functions. The first one $\mathcal{I}_\alpha(I)$ measures the damage caused by infection, and has a dependence in the total proportion of infected individual $I = \sum_\alpha \mathcal{N}_\alpha I_\alpha$ to include the consequence of the saturation of the sanitary systems once the epidemics goes beyond a certain level. The second one $f_\alpha(n_a^\gamma)$ measure the instantaneous cost for an individual a of class α due to the limitation of her contact, and depends one the “effort” n_a^γ made in each setting γ . Using Bellman linear programming, the optimal effort is given by Eq. (3.15),

$$n_a^{\gamma*}(t) = \underset{n_a^\gamma(t)}{\text{argmin}} [\lambda_a(t) (\mathcal{I}_\alpha(I(t)) - U_a(t)) + f_\alpha(n_a^\gamma(t))], \quad (4.4)$$

where the *individual force of infection* λ_a Eq. (3.6) is the analog of the global one λ_α Eq. (4.3) with the substitution $n_\alpha^\gamma \leftrightarrow n_a^\gamma$, and in which appears the *value function* $U_a(t)$, Eq. (3.10) determined by the HJB equation (3.14),

$$-\frac{dU_a(t)}{dt} = \min_{n_a^\gamma(t)} [\lambda_a(t) (\mathcal{I}_\alpha(I(t)) - U_a(t)) + f_\alpha(n_a^\gamma(t))]. \quad (4.5)$$

Finally, homogeneity of the population among each class leads to the additional requirement that one reaches a *Nash equilibrium*, i.e., that the optimal strategy of an individual a of class α corresponds to the global choice made on average by the class α lead to the self-consistent condition Eq. (3.16),

$$n_a^{\gamma*}(\cdot) = n_\alpha^\gamma(\cdot). \quad (4.6)$$

Equations (4.2)–(4.6) form the system of equations that need to solve to find the Nash equilibrium of our MFG problem.

B. Cost function and choice of the parameters

We turn now to the specific choice of parameters we will use in most of the following to illustrate the properties and

TABLE II. “Social-structure” and “biological” parameters used in our simulations. The matrix entries $\mathcal{M}_{\alpha\beta}^{\gamma(0)}$ correspond to the average frequency of contacts (per week) between an individual of age class α and someone of age class β in the setting γ . $\mathcal{N}_\alpha = N_\alpha^{\text{tot}}/N_{\text{tot}}$ is the proportion of the population in each age class. $I_\alpha(0)$ are the initial proportion of infected for each age class [we always assume $R_\alpha(0) = 0$]. ξ is the recovery rate (per week), ρ the transmission rate per contact, and μ corresponds to the proportion of asymptomatic individuals in the population. Finally, $\alpha = 1, 2, 3$ for age class of young, adults, and retired individuals, respectively. The way these parameters have been chosen is discussed in detail in Appendix B.

\mathcal{W}^S	\mathcal{W}^W	\mathcal{W}^C	\mathcal{W}^H
$\begin{pmatrix} 100 & 0 & 0 \\ 0 & 0 & 0 \\ 0 & 0 & 0 \end{pmatrix}$	$\begin{pmatrix} 0 & 0 & 0 \\ 0 & 75 & 0 \\ 0 & 0 & 0 \end{pmatrix}$	$\begin{pmatrix} 12.5 & 25 & 12.5 \\ 12.5 & 25 & 12.5 \\ 12.5 & 25 & 12.5 \end{pmatrix}$	$\begin{pmatrix} 15 & 25 & 10 \\ 12.5 & 32.5 & 5 \\ 10 & 10 & 30 \end{pmatrix}$
$\mathcal{N}_\alpha := N_\alpha^{\text{tot}}/N_{\text{tot}}$	$I_\alpha(0)$	(ξ, ρ, μ)	
(0.25, 0.5, 0.25)	(0.01, 0.01, 0.01)	(1.2, 0.1, 0.2)	

operational properties of our MFG model. In practice we need essentially to make a choice, on the one hand, for the “social-structure” and “biological” parameters of Table I (or their rescaled version introduced in Sec. IV A), and, on the other hand, for the functions $\mathcal{I}_\alpha(I)$ and the $f_\alpha(n_a^\gamma)$ of the cost (3.1), and the associated “cost-function” parameters.

For the former set of parameters, there is a fairly large scientific literature devoted to their evaluation from field data in specific, real-world situations. However, as noted above, our goal is not to model a particular instance of epidemic dynamics, but rather to illustrate the kinds of questions that can be addressed and the kinds of behaviors that can typically be obtained within our formalism. We have therefore chosen parameter values that we consider “generic,” relying on a number of studies [1,38,47–50] that analyze real epidemiological datasets. This approach makes it possible to evaluate the performance of the model under conditions that closely reflect practical scenarios, and allows us to expect that our model will produce comparable results in realistic applications. The exact way the “social-structure” and “biological” parameters were chosen is detailed in Appendix B, and their values is summarized in Table II.

Turning now to the cost (3.1), we take, for the cost of infection,

$$\mathcal{I}_\alpha(I(t)) = \tau_{1,\alpha} \exp \left[q_{\text{sat}} \frac{I(t) - \mathcal{J}_{\text{sat}}}{\mathcal{J}_{\text{sat}}} \right]. \quad (4.7)$$

This function includes the effect of a possible saturation of health services, and we assume an exponential increase of the strain on human and material resources as the saturation threshold \mathcal{J}_{sat} is approached, with a slope q_{sat} corresponding to the impact of saturation on the cost. As $I \ll \mathcal{J}_{\text{sat}}$, or $q_{\text{sat}} \rightarrow 0$, \mathcal{I}_α approaches an (age-class-dependent) constant $\tau_{1,\alpha}$ which implements the possibility that retired individual might be put significantly more at risk by the infection that younger ones. In practice we shall write these constants as $\tau_{1,\alpha} = \tau_1 \kappa_\alpha$, and keep the age-class-dependent part κ_α fixed for all our simulations, while in some instance exploring the changes due to the variations of τ_1 .

Turning now to $f_\alpha(n_a^\gamma)$, the cost of modifying social contacts, we choose to follow the same form as Turinici *et al.* in Ref. [32], namely,

$$f_\alpha(n_a^\gamma(t)) = \sum_\gamma (n_a^\gamma(t)^{-m_\gamma} - 1), \quad (4.8)$$

where m_γ models the degree of “attachment” to the setting γ : for example it is usually easier to reduce contacts at work than inside families. Moreover, f is decreasing with a positive second derivative, meaning that the more one decreases once social contacts, the higher the price to pay.

The set of values chosen in this section for the parameters characterizing the functions $\mathcal{I}_\alpha(I)$ and $f_\alpha(n_a^\gamma)$ is summarized in Table III. Finally, the parameter T denotes the time at which agents end their optimization process. This corresponds, for instance, to the time where herd immunity is reached, or it can depend on other circumstances such as the expected production of a vaccine, the seasonality of the virus, among others. In Sec. IV C, our simulations are performed on a duration of $T = 40$ weeks to focus on scenarios where collective immunity is reached and to avoid short end-time effects. Scenarios for which, due to short end-time, collective immunity is not reached at the end of the optimization period will be studied more specifically in Sec. V B. Since the main wave of the epidemic appears in the first 10 weeks, we often present the results on a duration of 15 weeks.

C. Epidemics dynamics

Solving the MFG equations of Sec. IV A for the set of parameters defined in Tables II and III yields the dynamics of S , I , and R . Technical detail about the numerical

TABLE III. “Cost-function” parameters associated with the function Eq. (3.1) chosen for our simulations. The cost of infection \mathcal{I}_α Eq. (4.7) is characterized, on the one hand, by its value under “normal circumstances” $\tau_{1,\alpha} = \tau_1 \kappa_\alpha$, where we distinguish a common coefficient τ_1 that will take different values depending on the simulation, and an age-dependent part κ_α , which we will keep fixed at the value given in this table. On the other hand, \mathcal{J}_{sat} characterizes the fraction of infected individuals at which the sanitary system starts to malfunction, and q_{sat} the speed at which this malfunction sets in. The cost of reducing once social contact is then parameterized by n_{min}^γ , the minimum contact willingness in each setting γ , and m_γ , which weights the cost of contact reduction in each setting. $\mathcal{J}_d, \mathcal{J}_l$ are the thresholds for the best lockdown and \mathfrak{s} its intensity level.

$(\mathcal{J}_{\text{sat}}, q_{\text{sat}})$	κ_α	m_γ	n_{min}^γ	$(\mathcal{J}_d, \mathcal{J}_l, \mathfrak{s})$
(0.1, 0.1)	(1,10,100)	(2,2,1,3)	$(\frac{1}{3}, \frac{1}{5}, \frac{1}{5}, \frac{1}{2})$	(0.12, $4 \cdot 10^{-4}$, 0.35)

implementation is given in Appendix D. The corresponding curves are displayed at the second line of Fig. 6.

The characteristic features of the Nash equilibrium are better revealed if one compares the corresponding epidemic dynamics with other scenarios. We shall consider the following options, which will be discussed in greater detail in the following subsections. We shall refer to the Nash equilibrium presented in Sec. IV D as the *unconstrained Nash equilibrium*. By contrast, the second scenario (see Sec. IV E) is a “*constrained*” Nash equilibrium, where individuals have to deal with global constraints imposed by an authority, for instance, a temporary lockdown which limits the agent’s strategy freedom, which translates into bounds on n_a . This second scenario divides into two subscenarios, depending on whether these constraints are naive or optimally chosen. A third scenario, discussed in Sec. IV F, is that of a *the societal optimum*, which is the idealistic case where everybody strives to optimize the global cost and chooses their strategy n_a accordingly. We call the “null” scenario *business as usual*: the agents do not adapt their behavior to the epidemics, so that no modification of the contact parameter is done, namely, n_a is fixed to 1. In each of these cases, the epidemic dynamics is driven by Eqs. (4.2)–(4.6), but with different $\{n_a^\gamma(\cdot)\}$, and thus different forces of infection $\{\lambda_\alpha\}$.

Solving the MFG equations in these different contexts leads to different dynamics for S , I , and R . The dynamics for each of the above scenarios is summarized in Fig. 6; the precise description of the scenarios is the object of the following subsections. As Fig. 6 shows, there are notable similarities between the different “optimized” scenarios (Nash, constrained Nash and societal optimum) and the business as usual one. For instance, the number of susceptible individuals at the end of the epidemic is $S_\infty \simeq 0.4$ in all cases but for the business as usual scenario, where it is significantly below (first row). This is due to the fact that in all circumstances one needs to reach herd immunity to escape from the disease, and the fact that S_∞ is much below this required value is a clear indication of the business as usual suboptimal character. In the same way, for all optimized scenarios there is a significant difference between the height of the infection wave for the different age class, as retired individuals and adults are more impacted by the disease than the youths, and therefore protect themselves. In the business as usual scenario the difference is much less significant, and only due to the relative proportion of contacts in each age class. However, the constrained Nash equilibrium with “naive” constraints differs from all the others because of the existence of two epidemic waves, which can be understood as originating from an excessive limitation of contacts that prevents the society from reaching herd immunity. Other differences, which are mainly quantitative, also exist between these different scenarios, and will be discussed in more details in Sec. IV G. We now turn to the detailed description of each scenario.

D. (Unconstrained) Nash equilibrium

Let us first consider the (unconstrained) Nash equilibrium. We have seen that it is described by two sets of differential equations. The first one is the rate equation of the epidemic, Eq. (4.2) (also known as the Kolmogorov equation in this

context), which is forward in time, that is, starting from initial conditions $S_\alpha(0), I_\alpha(0), R_\alpha(0)$, populations at later time t in age class α are obtained by solving Eq. (4.2) with $\lambda_\alpha(t)$ given by Eq. (4.3). The second set of equations corresponds to the Hamilton-Jacobi-Bellman equation (4.5), with one reference individual a for each age class α . As only the terminal condition on U is fixed, namely, $U_a(T) = 0$, Eq. (4.5) is backward in time. At equilibrium, all individuals will follow their own optimal strategy; but as all agents in a given age class are equivalent, this optimal strategy should be the same for all agents a of age class α . Thus we have the additional self-consistency condition Eq. (4.6), which imposes that if all other agents follow the strategy solution of the self-consistent system Eqs. (4.2), (4.5), and (4.6), deviating from that strategy implies a higher cost. The solution of the MFG equation thus corresponds to a Nash equilibrium.

The two equations (4.2) and (4.5), together with the self-consistency condition (4.6), form a system of equations coupling all epidemic rates $S(\cdot), I(\cdot), R(\cdot)$ and all age-class strategies n_a^γ via the individual optimal strategies $n_a^{\gamma*}$. Indeed, the epidemic rates in Eq. (4.2) depend on $\lambda_\alpha(t)$ given in Eq. (4.3), which depend on the global strategies n_β^γ . In turn, the optimal strategy $n_a^{\gamma*}$ for a reference individual a is a solution of HJB equation (4.5). With the precise form of the costs $\mathcal{I}_\alpha(I(s))$ and $f_\alpha(n_a^\gamma(t))$ chosen in Sec. IV B, it can be computed explicitly and reads

$$n_a^{\gamma*}(t) = \left(\frac{\mu\rho}{m_\gamma} [\mathcal{I}_\alpha(I(t)) - U_a(t)] \sum_{\beta=1}^{n_{cl}} n_\beta^\gamma(t) \mathcal{M}_{\alpha\beta}^{\gamma(0)} I_\beta(t) \right)^{-\frac{1}{m_\gamma+1}}, \quad (4.9)$$

which depends on the global strategies $n_\beta^\gamma(\cdot)$ explicitly, and implicitly through the epidemic rate $I(\cdot)$. One obtains in this way an initial-terminal value problem, which can be solved numerically in different ways; we present some of them briefly in Appendix D 1.

The solutions of the MFG system (4.2)–(4.6) are displayed in the second row of Fig. 6 for the set of epidemics quantities $S_\alpha(\cdot), I_\alpha(\cdot), R_\alpha(\cdot)$, and in Fig. 7 for the set of optimal strategies $n_a^\gamma(\cdot)$. For our choice of parameters, young individuals do not modify at all their behavior, when retired people reach maximal effort for significant amount of time in both community and household settings, and adults do some efforts, but without ever reaching the maximum one.

E. Nash equilibrium under constraints

In the Nash equilibrium considered above, each agent optimises for herself, and the resulting Nash equilibrium can lead to a global cost for the society,

$$C_{\text{glob}}(\{n_\beta\}) \equiv \sum_{\alpha} \mathcal{N}_\alpha C_\alpha(n_a = n_\alpha, \{n_\beta\}), \quad (4.10)$$

which is suboptimal. In Eq. (4.10), $\{n_\beta\}$ is the set of strategies followed by each age class, $n_a = n_\alpha$ means that any given individual a of class α follows the strategy n_α assigned to age class α , and the cost for each age class is weighted by the proportion \mathcal{N}_α of individuals in that class. A question that naturally arises from a public policy point of view is to

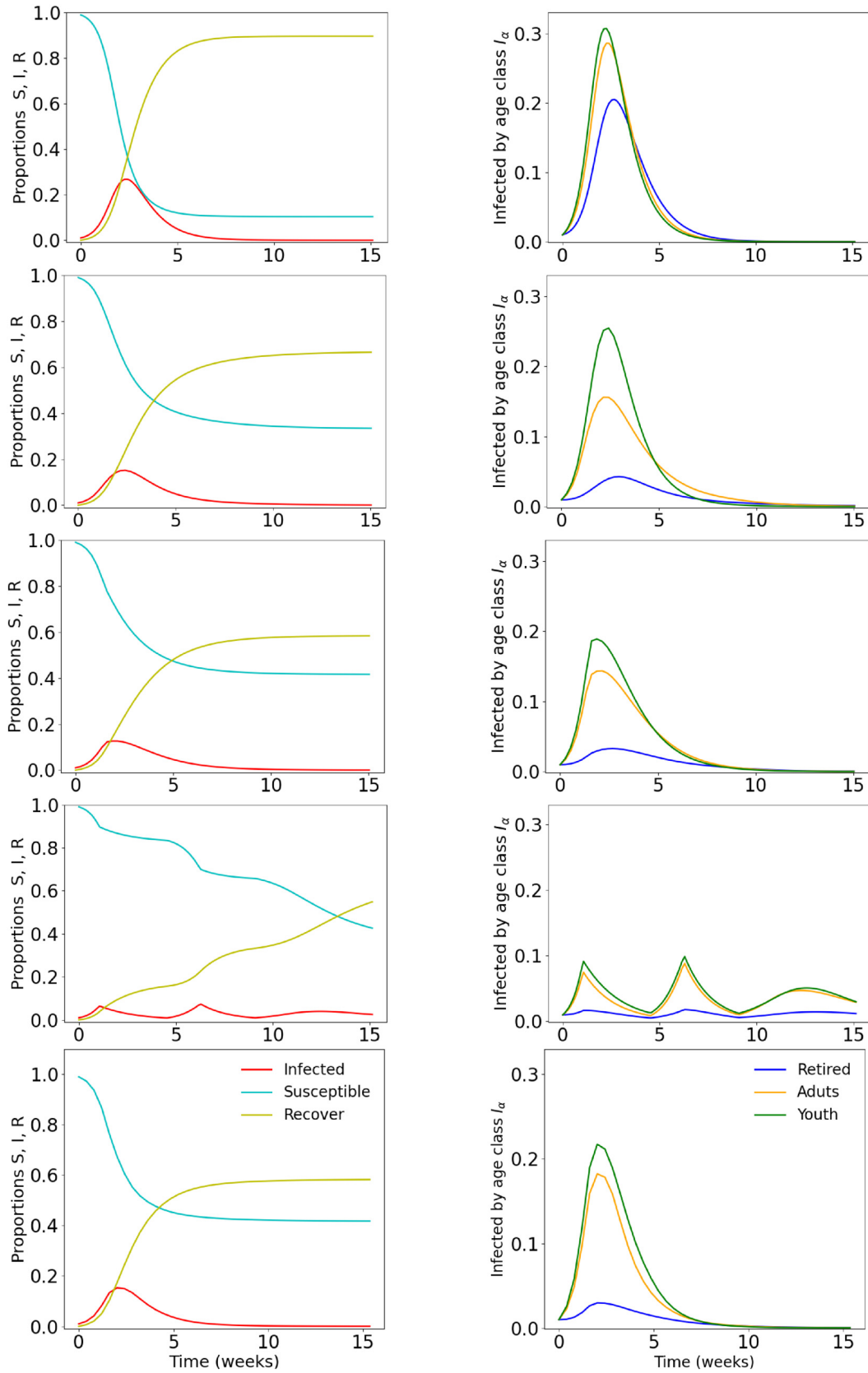


FIG. 6. Time evolution of the epidemic quantities with $\tau_1 = 1$ and parameters of Tables II and III. From top to bottom: Business as usual (no efforts), (unconstrained) Nash equilibrium, Nash equilibrium under optimal constraints, Nash equilibrium with naive constraints, societal optimum. Left: Time evolution of the proportion of susceptible S (cyan), infected I (red), and recovered R (yellow) in the population. Right: Time evolution of the proportion of infected in each age class I_α , retired people are in blue, adults in orange, and youth in green.

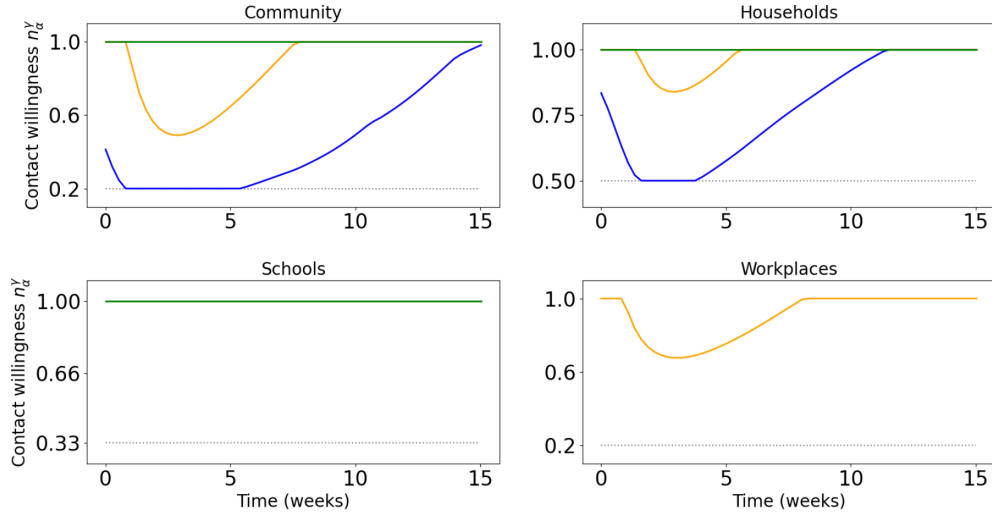


FIG. 7. Time evolution of the contact willingness $n_{\alpha}^{\gamma}(t)$ with $\tau_1 = 1$ at the Nash equilibrium. We plot $n_{\alpha}^{\gamma}(t)$ for each type of individual according to their age class (retired people in blue, adults in orange and youth in green) in community (upper left), households (upper right), schools (lower left, for the young) and workplaces (lower right, for the adults). The dotted gray horizontal lines correspond to the minimum contact willingness allowed (maximum effort).

know whether one could improve the global wellbeing of the population by driving the position of the Nash equilibrium through constraints on the population. This is, in some sense, what has been attempted in many countries during COVID-19 pandemic. The restrictions taken then, however, involved a lot of guesswork, both about the precise decisions to take, and about their potential effects on society (individuals behavioral response, impact on economic, health, etc.).

Here we present a possible quantitative approach to study such restriction policies, which aim at reducing the societal cost by constraining the behavior of individuals. Again, we remain here at the level of a “proof of concept,” as practical implementations of our formalism would require determining realistic forms of the cost functions and of the constraints, which is clearly beyond the scope of our work.

With the free (i.e., unconstrained) Nash equilibrium, individuals choose their contact willingness $n_{\alpha}^{\gamma}(t)$ in the range $[n_{\alpha,\min}^{\gamma}, 1]$, where the maximum 1 correspond to the situation without epidemic. We now add a constraint similar to a partial lockdown, by setting this maximum to $n_{\alpha,l}^{\gamma} < 1$ when some epidemic level is reached. In that way, everyone is required to make a minimal amount of efforts to preserve the sanitary system and reduce the societal cost (4.10). This “lockdown” is implemented when the proportion of infected $I(t)$ reaches a certain threshold \mathcal{J}_d , and, as the proportion of infected decreases we assume the lockdown is lifted when $I(t)$ goes below a value $\mathcal{J}_1 < \mathcal{J}_d$ (which is assumed lower than \mathcal{J}_d to avoid unrealistic oscillations around \mathcal{J}_d). The lockdown has thus a hysteresis form, and is implemented in the following way (with L a Boolean variable which is 1 if the lockdown is active and 0 otherwise):

$$\begin{aligned}
 & \text{if } I(t) < \mathcal{J}_1 : n_{\alpha}^{\gamma}(t) \in [n_{\alpha,\min}^{\gamma}, 1] \quad \& \quad L \mapsto 0 \quad \text{no constraints,} \\
 & \text{if } I(t) > \mathcal{J}_d : n_{\alpha}^{\gamma}(t) \in [n_{\alpha,\min}^{\gamma}, n_{\alpha,l}^{\gamma}] \quad \& \quad L \mapsto 1 \quad \text{active constraints,} \\
 & \text{if } \mathcal{J}_1 < I(t) < \mathcal{J}_d \text{ and } L = 0 : n_{\alpha}^{\gamma}(t) \in [n_{\alpha,\min}^{\gamma}, 1] \quad \text{no constraints,} \\
 & \text{if } \mathcal{J}_1 < I(t) < \mathcal{J}_d \text{ and } L = 1 : n_{\alpha}^{\gamma}(t) \in [n_{\alpha,\min}^{\gamma}, n_{\alpha,l}^{\gamma}] \quad \text{active constraints.}
 \end{aligned} \tag{4.11}$$

In Eq. (4.11), we choose $n_{\alpha,l}^{\gamma} = \varepsilon n_{\alpha,\min}^{\gamma} + (1 - \varepsilon)$, with $\varepsilon \in [0, 1]$ a variable measuring the intensity of the lockdown: $\varepsilon = 0$ corresponds to the free situation without any constraint, while $\varepsilon = 1$ corresponds to a strict lockdown with no freedom, as $n_{\alpha}^{\gamma}(t)$ is fixed to $n_{\alpha,\min}^{\gamma}$. Therefore, the lockdown is described by a set of three variables ($\varepsilon, \mathcal{J}_d, \mathcal{J}_1$): the intensity ε , the first threshold \mathcal{J}_d , and the second threshold \mathcal{J}_1 . The numerical implementation of this set of equations is briefly discussed in Appendix D 2.

In Fig. 6 (third row) we show the evolution of the epidemic quantities for the choice of parameters ($\varepsilon = 0.35, \mathcal{J}_d =$

0.12, $\mathcal{J}_1 = 4.10^{-4}$). As shown in Appendix E this choice corresponds to an optimal value in the sense that these parameters minimise the global cost Eq. (4.10) among all possible constraints in the parameter space ($\varepsilon, \mathcal{J}_d, \mathcal{J}_1$). In Fig. 8 we display the corresponding strategies chosen by individuals under these constraints. The constraints are enforced after 2 or 3 weeks into the epidemic, and are raised after almost 14 weeks (over 40 for the total epidemic time) when the proportion of infected is low and there is no risk of any epidemic rebound. The values of the constraints appear as straight lines followed by youth individuals, whose behavior is not dictated by their own

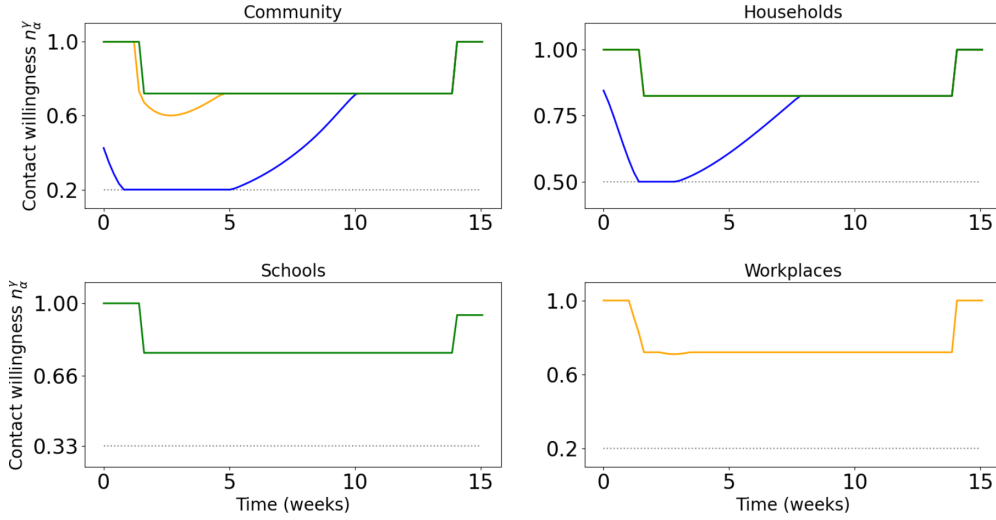


FIG. 8. Time evolution of the contact willingness $n_\alpha^\gamma(t)$ with $\tau_1 = 1$ for the Nash equilibrium under optimal constraints ($\varepsilon = 0.35$, $\mathcal{J}_d = 0.12$, $\mathcal{J}_1 = 4.10^{-4}$). We plot $n_\alpha^\gamma(t)$ for each type of individual according to their age class (retired people in blue, adults in orange and youth in green) in community (upper left), households (upper right), schools (lower left, for the young) and workplaces (lower right, for the adults). The dotted gray horizontal lines correspond to the minimum contact willingness allowed.

“egoistic” optimisation but by the fact they are forced to respect the lockdown as soon as it is imposed. Retired people, however, choose most of the time to limit their contact even more than required by the constraints; adults most of the time just follow the lockdown, but sometimes limit their contacts further.

As we shall discuss in Sec. IV G this optimal lockdown, despite the fact that it depends on only three parameters, can improve on the free Nash equilibrium, in the sense that the societal cost Eq. (4.10) is lower. However, public policies executives have to be careful about their choice as it can generate situations which are clearly worse than the free Nash equilibrium. We illustrate this situation in Figs. 6 (fourth row) and 9 with parameters ($\varepsilon = 0.8$, $\mathcal{J}_d = 0.06$, $\mathcal{J}_1 = 0.01$): in that case

one imposes a very strong but short lockdown. Since we consider here a long end-time configuration with $T = 40$ weeks, for which collective immunity is required to end the epidemic, this leads to epidemic rebounds and increases significantly the epidemic cost. Indeed, all drastic efforts that are made while the epidemic is low, and before collective immunity is obtained, are essentially useless, and just add to the global cost endured by the population. In what follows we shall thus distinguish Nash under optimal constraints (NOC) and Nash under “naive” (uncarefully chosen) constraints (NNC).

F. Societal optimum

In the previous two scenarios, each agent performs a personal, possibly constrained, but essentially egoistic,

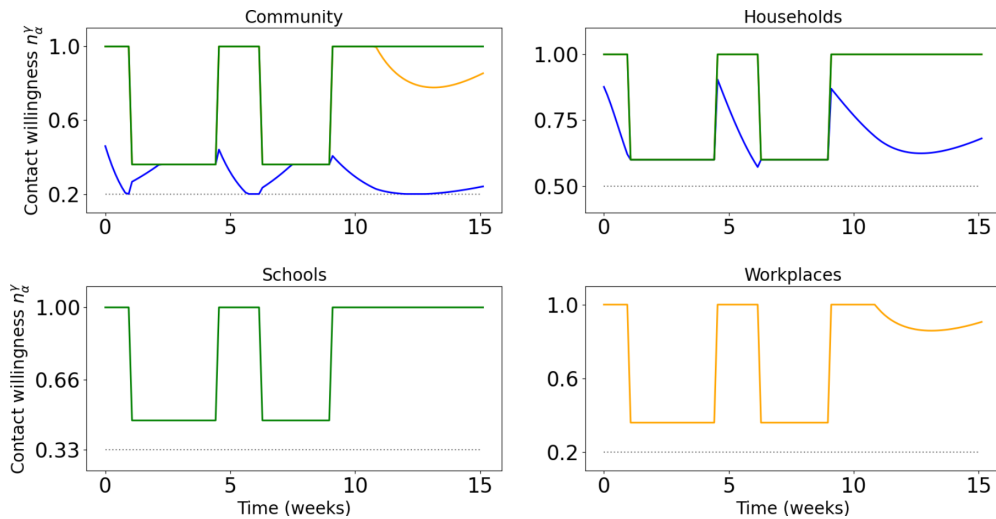


FIG. 9. Time evolution of the contact willingness $n_\alpha^\gamma(t)$ with $\tau_1 = 1$ for the Nash equilibrium under naive constraints ($\varepsilon = 0.8$, $\mathcal{J}_d = 0.06$, $\mathcal{J}_1 = 0.01$). We plot $n_\alpha^\gamma(t)$ for each type of individual according to their age class (retired people in blue, adults in orange and youth in green) in community (upper left), households (upper right), schools (lower left, for the young), and workplaces (lower right, for the adults). The dotted gray horizontal lines correspond to the minimum contact willingness allowed.

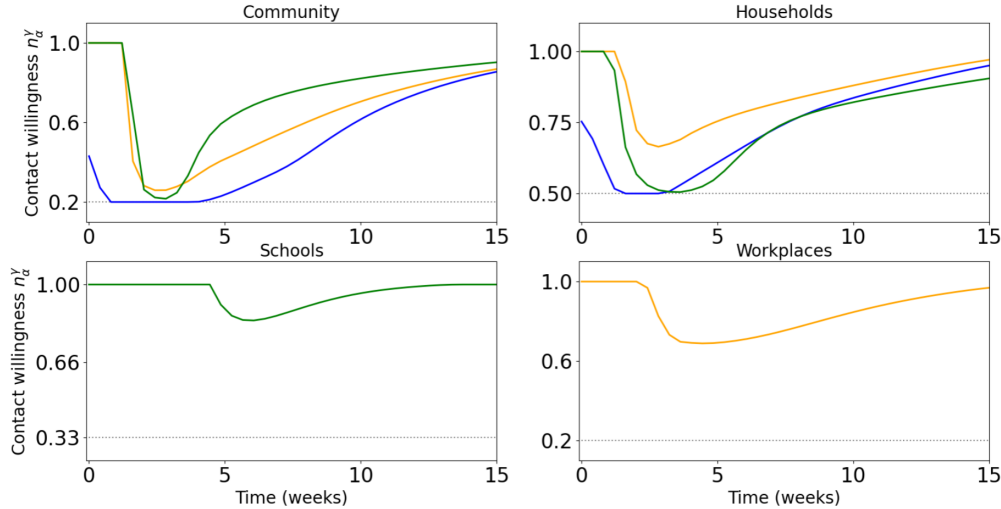


FIG. 10. Time evolution of the contact willingness $n_{\alpha}^c(t)$ with $\tau_1 = 1$ for the societal optimum. We plot $n_{\alpha}^c(t)$ for each type of individual according to their age class (retired people in blue, adults in orange and youth in green) in community (upper left), households (upper right), schools (lower left, for the young), and workplaces (lower right, for the adults). The dotted gray horizontal lines correspond to the minimum contact willingness allowed.

optimization. To set the scale of what is the cost associated with these egoistic approaches, it may be useful to compare them with the “societal optimum” that could be imposed by a “benevolent global planner,” i.e., a well-meaning government with full empowerment. Considering the global cost, seen at the society level, as the addition of all individual costs, this amounts to finding the minima of the cost Eq. (4.10). There is already a rich literature on topics related to societal optimization (see, for example, Refs. [6,7,32,51–57]) on various types of models, as this problem is reduced to a single global optimization. The difference between this minimization and the Nash equilibrium discussed above is referred to as “the cost of anarchy”: while there is no cooperation between individuals in the Nash equilibrium, the societal optimum case corresponds to “the best” (from a societal cost point of view) that one can obtain for C_{glob} among all possible strategies.

The numerical construction of this societal optimum is briefly discussed in Appendix D3. In Fig. 6 (fifth row) we show the epidemic quantities associated with the societal optimum. However, the total number of infected individuals is not the lowest possible, as infection within the youths does not carry the same cost as within the retired agents. The total amount of infected at the end of the epidemic is still relatively high, because in our framework, one has to reach collective immunity to definitely escape from the disease. Also, the epidemic peak is still at a rather high level, as it is efficient to allow an epidemic spread while keeping the epidemic under control to reach quickly herd immunity. However, the precise distribution of infected proportion in each age class is different from the free Nash equilibrium.

In Fig. 10 we show the corresponding optimal contact willingnesses. They do not correspond to individual optimum; rather, there is a cooperation between individuals in different age classes to get an epidemic which will make lower damage with a reasonable amount of efforts. In the community setting and in households, we observe that all individuals make significant efforts during the epidemic peak to avoid a global

infection peak that would saturate the sanitary system: they do it in particular in those two settings to avoid a too strong diffusion to retired people. However, efforts are done with less intensity in schools and workplaces. Once the epidemic peak is reached, we see that the epidemic continues to spread, in particular in young and adults classes, so that collective immunity can be reached and in this way protect retired people. Thus, the efforts in schools and workplaces are here to smooth sufficiently the epidemic, avoid any rebound, and get a relative collective immunity as fast as possible, making it possible to lift the efforts in communities and households.

G. Comparison between the different scenarios

1. Comparison of global costs

To compare quantitatively the scenarios presented above, we normalize the costs with respect to the total cost of the societal optimum, which we set equal to 100.

In Fig. 11 we show, for the choice of parameters given in Tables II and III, the global costs obtained with the different kinds of scenarios considered above. As expected, the societal optimum (SO) is the best strategy at society level, followed quite closely by the NOC, which itself is better than the free Nash equilibrium (N). As the imposition of societal-optimal scenarios implies a lack of freedom for the individual, as well as a coordination cost which may be significant and which is not included in Eq. (4.10), we argue that the constrained Nash equilibrium presumably forms in practice a good compromise between effectiveness and practicability. One should bear in mind, however, that with a naive choice for the constraints, such as for the NNC strategy of Fig. 11, one could easily obtain a result worse than for the free Nash equilibrium.

The color bars in Fig. 11 illustrate the relative importance of each age class in the total cost paid by the society. This shows that, to reach a global optimum, the key point is to reduce as much as possible the cost for retired people whose contribution is large. This contribution is actually larger than

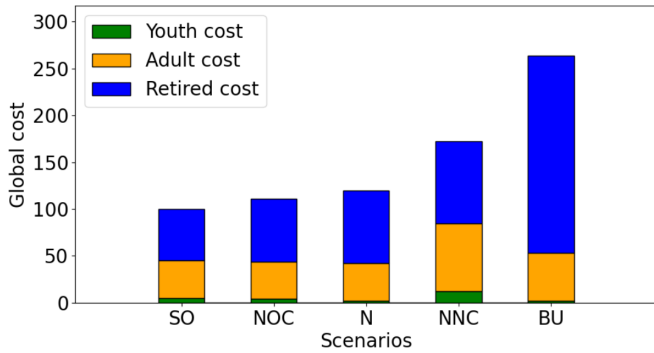


FIG. 11. Comparison of costs for the different scenarios studied: SO (societal optimum), NOC (Nash under optimal constraints), N (free Nash equilibrium), NNC (Nash under naive constraints), BU (business as usual). The costs are represented on a base of 100 for SO; the color bars represent the total cost of each age class. Thus, the level of each bar comes from the cost per individual multiplied by the proportion \mathcal{N}_a of his age class.

that of adults, despite the latter representing twice as many people as retired individuals in our population choice. Note that, from the point of view of adults or young people, the free Nash equilibrium is the best strategy, as they do not have to make efforts for others. We can also notice that making a wrong choice for the constraints will not lead to the same “extra cost” for everyone. Indeed, for the NNC scenario, the cost for retired people is still relatively low because the epidemic is maintained at a low level, but the cost of social restrictions becomes very high for adults and young individuals. This has to be contrasted with the business as usual scenario where the extra cost is borne almost exclusively by retired people.

2. Comparison of contact willingness for the two best scenarios

In Fig. 12, we show the comparison between the contact willingness obtained with the societal optimum (dashed line)

and the Nash equilibrium under optimal constraints (solid line). We see that for the Nash equilibrium under constraints we get constraints which start at almost the same time as the ones of the societal optimum (after typically 2 weeks); but since it is a Nash equilibrium, these constraints are raised after a long time, around 14 weeks, so that even without individual efforts from adults and youth the epidemic is kept under control. At a global level, these constraints are not too strong compared to the ones of the societal optimum, but since they are less localized, both spatially (in the good settings) and temporally (during the epidemic peak with a progressive release afterwards), they are less effective to protect retired people who suffer from a higher epidemic with a larger total number of infected people at the end of the epidemic.

These two scenarios, the societal optimum and the Nash equilibrium under constraints, suggest interesting guidelines for public health executives to mitigate an epidemic through collective immunity. First, quite naturally, sufficiently strong constraints should be imposed at the epidemic peak to avoid saturation of the sanitary system; and the constraints need to protect people at risk, which implies to limit contact both among these people as well as between the rest of the society and these individuals. However, in a perhaps less intuitive way, constraints on people who are not at risk should be relatively light. Indeed, the epidemic needs to spread on the population, in a controlled way, to reach as fast as possible the collective immunity. After the epidemic peak, one can lift progressively the constraints, until the collective immunity is reached. At this point, the epidemic will be back at a low level and will stay low while the constraints can be completely lifted. The precise characteristics of the constraints, such as their intensity or their timing, will depend on the characteristics of the population and of the disease under consideration. However, scenarios that induce epidemic rebound, like the Nash scenario with naive constraints described above, are quite ineffective in such a context, because the time span between the peaks does not help reaching collective

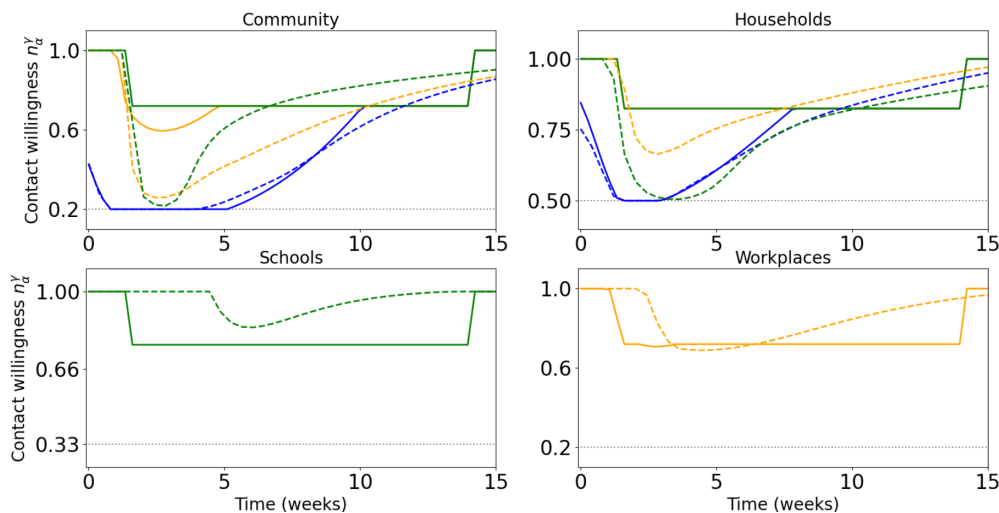


FIG. 12. Comparison of contact willingness for the societal optimum (dashed line) and the Nash equilibrium under optimal constraints (solid line). We plot $n_a^c(t)$ for each type of individual according to their age class (retired people in blue, adults in orange and youth in green) in community (upper left), households (upper right), schools (lower left, for the young) and workplaces (lower right, for the adults). The dotted gray horizontal lines correspond to the minimum contact willingness allowed.

immunity and is very costly in terms of constraints on the society.

V. OPTIMAL STRATEGIES FOR DEALING WITH AN EPIDEMIC FROM THE HEALTH AUTHORITY POINT OF VIEW

Up to this point, we have only considered dynamics with a very long end-time T , and a large number of agents N_{tot} , so that the only option to terminate the epidemic is to reach herd immunity. However there are many circumstances (expected production of a vaccine, seasonality of the virus which is expected to disappear in the summer, etc.) where the finiteness of T plays a role, and others (isolated geographic configuration such as islands, strict control of borders, etc.) where the finiteness of N_{tot} does. This opens the way to other possible strategies, from the point of view of the centralized health authority, to control the epidemics. We review them in this section.

A. Threefold way of controlling an epidemic

Based on these considerations, we can identify three possible ways to deal with an epidemic: reach collective immunity (typically for T, N large), contain the epidemic (for T small), or eradicate the epidemic (for N_{tot} small). We characterize these three ways as follows.

1. Strategy No. 1: Reach collective immunity

This is the strategy that was implicitly used in the previous sections since we assumed both T and N_{tot} very large. More formally, we consider that collective immunity has been reached at time t if the proportion of infected individuals is a decreasing function of time for $t' > t$ even in the absence of efforts after t . For the basic SIR model Eq. (2.1) with constant χ , let $R_{\text{eff}}(t) = S(t)R_0$ be the effective reproduction number at time t , that is, the average number of secondary infected caused by a single infected agent, with $R_0 = \rho\chi/\xi$ the initial value of R_{eff} when $S = 1$. For this model we have $\dot{I}(t) = \xi I(R_{\text{eff}}(t) - 1)$. In this case, collective immunity is reached as soon as $R_{\text{eff}}(t) < 1$ since S is decreasing. In a similar way, for our compartmental model we introduce

$$R_\alpha(t) = \frac{\mu\rho}{\xi} \sum_{\beta,\gamma} n_\alpha^\gamma(t)n_\beta^\gamma(t)\mathcal{M}_{\alpha\beta}^\gamma S_\beta(t), \quad (5.1)$$

the average number of secondary infected caused by a single infected agent of age class α . We stress that $R_\alpha < 1$ does not imply $\dot{I}_\alpha < 0$, since the number of infected in the age class α involves the R_β of all classes, and some of them may be greater than 1. However, if *all* the R_α are less than one, then the average proportion of infected individuals, $I \equiv \sum_\alpha \mathcal{N}_\alpha I_\alpha$ can be easily shown to be a decreasing function. Indeed, from Eq. (2.12), we have $\dot{I} = \sum_\alpha \mathcal{N}_\alpha S_\alpha \lambda_\alpha - \xi I$, and

$$\begin{aligned} \sum_\alpha \mathcal{N}_\alpha S_\alpha \lambda_\alpha &= \mu\rho \sum_{\beta,\gamma,\alpha} \mathcal{N}_\alpha S_\alpha n_\alpha^\gamma(t)n_\beta^\gamma(t)\mathcal{M}_{\alpha\beta}^\gamma I_\beta \\ &= \xi \sum_\beta \mathcal{N}_\beta I_\beta R_\beta, \end{aligned} \quad (5.2)$$

where we used the sum rule $\mathcal{M}_{\alpha\beta}\mathcal{N}_\alpha = \mathcal{M}_{\beta\alpha}\mathcal{N}_\beta$ enforced by the symmetric nature of contacts. We therefore have

$$\dot{I} = \xi \sum_\alpha \mathcal{N}_\alpha I_\alpha (R_\alpha - 1). \quad (5.3)$$

In the absence of effort, the rates $R_\alpha(t)$ become $R_\alpha^{(0)}(t) = \frac{\mu\rho}{\xi} \sum_{\beta,\gamma} \mathcal{M}_{\alpha\beta}^\gamma S_\beta(t)$, and Eq. (5.3) becomes

$$\dot{I}^{(0)} = \xi \sum_\alpha \mathcal{N}_\alpha I_\alpha (R_\alpha^{(0)} - 1), \quad (5.4)$$

where the superscript denotes the absence of effort. Since the $R_\alpha^{(0)}$ are obviously decreasing functions of time, the constraint that $R_\alpha^{(0)}(t) < 1$ for all age classes α is a sufficient, but not necessary, condition to have reached herd immunity. This constraint is, however, too strong, and is actually not met in our simulations, even when herd immunity is achieved. We thus find more effective to replace it by a heuristic condition obtained by assuming the I_β to be not very different from the average I (as can be seen for example in Fig. 6 towards the end of the epidemics). Using Eq. (5.4), we get $\dot{I}^{(0)} \simeq \xi I(R^{(0)} - 1)$, with

$$R^{(0)} \equiv \sum_\alpha \mathcal{N}_\alpha R_\alpha^{(0)}. \quad (5.5)$$

$R^{(0)}$ is also a decreasing function of time, and the heuristic criterion $R^{(0)}(t) < 1$ indicates that herd immunity has been reached at t . This empirical condition does not guarantee mathematically the absence of an epidemic rebound once $R^{(0)}(t) < 1$ (heterogeneous I_α could allow $\dot{I}^{(0)} > 0$). Nevertheless, we will check below numerically that for the cases we considered it does actually correspond to herd immunity [58]. This strategy, where S needs to be low at the end of the epidemics, is often used for moderate epidemics and for epidemics where no other strategy is available.

2. Strategy No. 2: Contain the epidemic

If an external event (e.g., vaccine) is expected to end the epidemic within a relatively short time, then another possibility to deal with an epidemic is to contain it during the period of optimization T , keeping the epidemic at a low level, and end at T with a number of susceptible far above the collective immunity threshold. In practice, we are in this phase if $R^{(0)}(T) > 1$. This is the strategy adopted by most countries during the COVID-19 pandemic: hold on and contain the epidemic until a vaccine is available.

3. Strategy No. 3: Eradicate the epidemic

A final possibility is to act on the epidemic sufficiently early and sufficiently intensely, that one will be able to eradicate it before it spreads to the general population. To implement such an idea, we need to assume a finite size N_{tot} of the population, and state that below a certain rate of infected, of order $1/N_{\text{tot}}$, the epidemic vanishes or is at least under control so that there is no propagation anymore. Of course in practice, one would need to know precisely who is infected and insulate them from the rest of the population (by keeping them in quarantine at hospital, for instance), which would induce an extra cost of coordination which is not taken into account here. Discussing this strategy requires to add

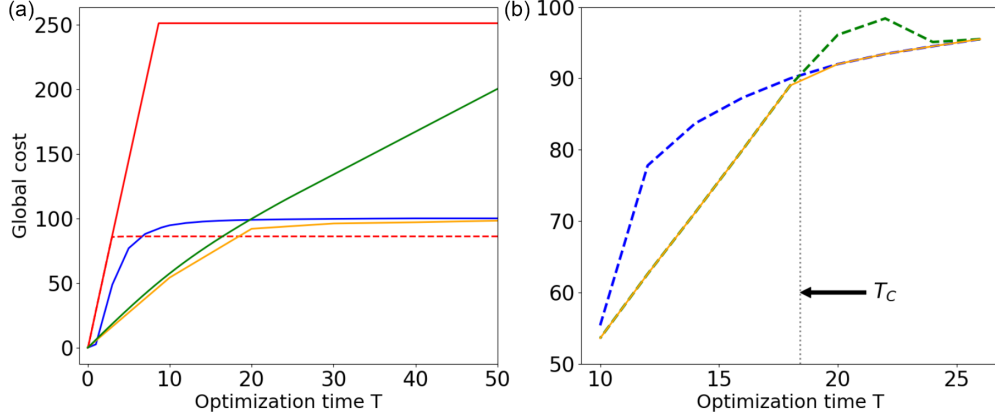


FIG. 13. (a) Comparison of the evolution of the global cost $C_{\text{glob}}(n, T)$ for the three template strategies n_{im} (blue line), n_{era} (red lines), n_{cont} (green line) which are well defined for any value of t (from 0 to ∞). For the global cost associated to the eradication strategy n_{era} (in red) we take, respectively, $I_{\text{thr}} = 1.10^{-5}$ (respectively, $I_{\text{thr}} = 1.10^{-3}$) for the solid line (respectively, dotted line). Regarding the strategy n_{im} , $T = \infty$ is approximated here by $T = 100$. Finally, in orange, we plot the true societal optimum cost at T (with $I_{\text{thr}} = 1.10^{-5}$, solid line parameters). (b) Evolution of the global cost of the societal optimum (orange solid line) close to the transition time T_c (see text). Dotted blue (respectively, green) line: evolution of the global cost with a continuous change of the strategy n for the herd immunity scenario (respectively, containment scenario). Details of the computation are explained in the main text.

one parameter, I_{thr} , which corresponds to the threshold at which we consider that the epidemic vanishes, with a value for I_{thr} of order $1/N_{\text{tot}}$. This approach is in practice possible only during the early stages of the epidemic, otherwise it will induce a considerable cost. This strategy has been used many times in China and some insular countries during COVID-19 pandemic, with strong restrictions at the early stages of the epidemic to avoid a massive spreading.

B. Template strategies

The above scenarios can be classified according to whether $\dot{I}^{(0)}(t) < 0$, $\forall t > T$ (herd immunity), and if this is not the case, whether $I(T) > I_{\text{thr}}$ (containment) or $I(T) < I_{\text{thr}}$ (eradication). Thus, any set of strategies $n(\cdot) \equiv \{n_{\beta}^{\gamma}(\cdot)\}$ (i.e., defined for each age class, in each setting, and all times t) belongs to one and only one of these classes. We can, however, do a little bit more than this formal classification, and introduce for each of these scenarios what we will call a “template strategy,” that is, a set of strategies $n(\cdot)$ which provides a good approximation to the optimal one within a given scenario. These “templates” can be defined as follows:

(1) *Reach collective immunity* n_{im} : Our template for the herd immunity scenario is defined as the optimal strategy defined in Sec. IV F taken in the limit $T \rightarrow \infty$ (with $I_{\text{thr}} \equiv 0$), namely,

$$n_{\text{im}}(\cdot) = \underset{n(\cdot)}{\operatorname{argmin}}[C_{\text{glob}}(n(\cdot), T \rightarrow \infty)]. \quad (5.6)$$

Indeed, we can expect that when the best approach is to use herd immunity, there is little end-time effect and the optimal strategy for a finite T will be quite close to the one corresponding to $T \rightarrow \infty$. As seen in Fig. 13, the global cost associated with n_{im} rises quite significantly at the beginning of the epidemic, as a significant number of agents assume the cost of infection, but once herd immunity is reached this cost flattens out since infection decreases while no effort is required anymore. It can be noted furthermore that n_{im} does not

depend much on τ_1 , as it minimizes the cost due to social contacts (which is independent from τ_1), while reaching collective immunity. This leads in first approximation to a constant number of agents who have been infected at the end time T , as the collective immunity threshold is unchanged for any value of τ_1 . Therefore, the associated final cost of this strategy n_{im} grows with a form $C_{\text{glob}}(n_{\text{im}}) \simeq F_{\text{tot}}(n_{\text{im}}) + (S_0 - S_{\infty})\tau_1$, where F_{tot} is the total amount of efforts made by agents for a strategy $n(\cdot)$, which is (almost) independent of τ_1 , and the second term grows linearly with τ_1 .

(2) *Contain epidemic* n_{cont} : We define the reproduction factor R as the $R^{(0)}$ which was introduced in Eq. (5.5), with here arbitrary value for $n(t)$ instead of 1. One can easily claim that a sufficient condition to strictly contain the epidemic in a homogeneous infected population is to keep $R(t) = 1$. With that condition, one will enforce $I(t)$ to stay at the same level or below the initial condition $I(0)$ with *a priori* the lowest possible cost from the social point of view [to keep $R(t) < 1$ will be more expensive]. We can therefore define the template strategy of the containment scenario as the one coming from the optimization

$$n_{\text{cont}}(t) = \underset{n(\cdot)}{\operatorname{argmin}}[F_{\text{tot}}(n(\cdot)) \text{ such that } R(t) = 1] \quad \forall t, \quad (5.7)$$

where we furthermore assume that for all age classes $S_{\alpha}(t) \simeq S_{\alpha}(0) \simeq 1$, so that n_{cont} is actually time-independent. Since the social cost only involves current time t , the problem reduces to a simple, local in time, optimization problem, where $n(t)$ becomes a constant n which must respect $R = 1$ and minimize $f(n)$. The result of this optimization, obtained numerically through a gradient descent under constraints, is illustrated in Fig. 13. Note that this (constant) strategy n_{cont} is independent of τ_1 , and the associated global cost $C_{\text{glob}}(n_{\text{cont}}) \simeq T f(n_{\text{cont}})$ is essentially independent of τ_1 and grows linearly with T .

(3) *Eradicate epidemic* n_{era} : For this case, it can be shown (see Appendix F) that, for the parameters we consider, the optimal eradication strategy is always obtained by an

application of the maximal effort until the time t_{thr} corresponding to the eradication of the epidemics, $I(t_{\text{thr}}) \equiv I_{\text{thr}}$. This strategy, will be taken as our template eradication strategy. The associated final cost is therefore expected to be of the form $C_{\text{glob}}(n_{\text{era}}) \simeq T f_{\text{max}}$ if $T < t_{\text{thr}}$, the cost grows linearly with T , and $C_{\text{glob}}(n_{\text{era}}) \simeq f_{\text{max}} t_{\text{thr}}$ if $T > t_{\text{thr}}$, where f_{max} denotes the social cost (rate) associated with a maximum amount of efforts and t_{thr} mainly depends on I_{thr} .

C. Phase transition

For these three scenarios, we show on Fig. 13(a) the evolution of the global cost with the optimization time T , for $\tau_1 = 1$ and the parameters of Tables II and III. As expected, all costs increase with T , but in different ways. In blue, the collective immunity cost grows rapidly at the beginning of the epidemic, so that collective immunity is reached as soon as possible without saturating the sanitary system, after which the cost levels up. For the containment strategy n_{cont} (green), we see that the corresponding cost increases almost perfectly linearly, as the amount of effort due to contact reduction is constant. As $S(0) = 0.99 < 1$, there is in this scenario a small spread of the infection at the beginning of the epidemic (and thus a small additional infection cost), before it vanishes completely. Finally, the cost of the eradication strategy (red curve) starts with a strong linear increase (the slope of the curve here is clearly higher than the one of the containment strategy since the maximal effort is applied), and then saturates at a level which depends on the threshold I_{thr} . Figure 13(a) also shows the societal optimum cost (orange curve), which always closely follows one of the templates. At low T , it is a bit below the cost of the containment strategy n_{cont} , taking advantages of end-time effects (as illustrated in Fig. 14) to slightly reduce the cost. For large T , it follows, again from below, the collective immunity template. For the societal optimum cost, there is a transition around 20 weeks for our choice of parameters, from a ‘‘containment’’ cost to a ‘‘collective immunity’’ cost. For $I_{\text{thr}} = 10^{-3}$ (dotted line in Fig. 13), the transition would go from ‘‘containment’’ to ‘‘eradication’’.

This transition between different scenarios’ costs strongly suggests that the associated strategies will follow the same pattern, with a transition from the neighborhood of n_{cont} to the neighborhood of n_{im} . To assess this, we compare in Fig. 14 the optimal strategy found from the societal optimum scenario with the template strategies. We observe that the small gap between template costs and societal optimum cost which was observed on Fig. 13(a) corresponds to a small difference between the corresponding strategies. For strategy 1 (rows 1 and 2) we observe a finite- T effect: an additional amount of efforts around 10 to 25 weeks appears to be profitable to limit the number of infected, even though the epidemic is almost over. The structure of the two strategies is nevertheless very similar. Regarding the ‘‘containment’’ strategy (rows 3 and 4), in each setting the contact willingness of each age class of agents is the same (thereby, only one constant dotted line per setting is plotted). The societal optimum is very close to the strategy n_{cont} , but two effects make it deviate from the idealistic strategy n_{cont} . First, as $S(0)$ is not strictly equal to one (here 0.99), there is some moderate spreading of the epidemics, which induces a small increase of effort from retired people,

as well as a small increase of infection cost. Second, there is a clear end-time effect, meaning here that individuals who are not at risk reduce their efforts just before T since epidemic will not have time to propagate massively until T (one can think of a vaccination campaign where individuals will start increasing their contacts before the campaign is completed). Note however that as T gets close, since the epidemic begins to grow, retired individuals protect themselves and actually further limit their contacts. Last, for the eradication strategy, the societal optimum is the same as our template strategy n_{era} (see Appendix F for more details).

Figures 13(a) and 14 indicate that our template strategies provide an accurate approximation of the societal optimum at small and large T . One question we may ask now is whether the transition we see at $T_c \simeq 20$ from one scenario to another can be understood as a true phase transition, or is rather of a crossover type. To address this question, in Fig. 13(b) we compare the societal optimum near T_c , i.e., the absolute minimum of the global societal cost, with the result of a gradient descent obtained in the following way: starting from above T_c (blue) or below (green), we change T by small steps δT , and use as a starting point for the gradient descent at $T + \delta T$ the result of the calculation at T . What we observe is that doing this procedure, our algorithm finds, for a significant range of T values around T_c a local minimum which follows the herd-immunity template below T_c (dotted blue) or the containment template above T_c (dotted green). This local minimum corresponds either to the true minimum when the blue or green curves match the orange one, and to a metastable state when they do not. Note that both local minima eventually fall to the global minimum (in orange) when they are sufficiently far from T_c , ending in a hysteresis cycle.

There is therefore a discontinuous change of the optimal strategy at T_c , which is the signature of a first-order phase transition. In this analogy with thermodynamics, the cost C_{glob} represents the free energy, and T some macroscopic parameter such as temperature. The Ehrenfest classification, which defines a first-order phase transition as a discontinuity of the first derivative of C_{glob} with respect to T at T_c , is clearly observed in Fig. 13(b). We expect this phase transition to exist for a large range of parameters of our model, and we have verified its existence numerically on a number of cases. In particular, we have checked that the transition between ‘‘containment’’ phase and ‘‘eradication’’ phase is also first-order.

We therefore end up with three distinct phases for the societal optimum, which exhibit first-order phase transitions between them, and which are well-approximated by template strategies defined above. Since these template strategies provide good approximations of the societal optimum one, we use them in Fig. 15 to show the ‘‘phase diagram’’ of the optimal scenarios as a function of the optimization time T and the infection cost τ_1 . Of course, the optimal strategy will depend on all the parameters that we have introduced until now, but some of them (matrix of contacts \mathcal{M} , capacity of the sanitary system q_{sat} , proportion of agents in each age class \mathcal{N}_α) may be assumed to be quite similar for different epidemics affecting the same population, while T and τ_1 depend a lot on the virus under consideration and have a major impact on the best strategy. The three different scenarios appear to be optimal in distinct well-defined areas of the phase diagram. When T

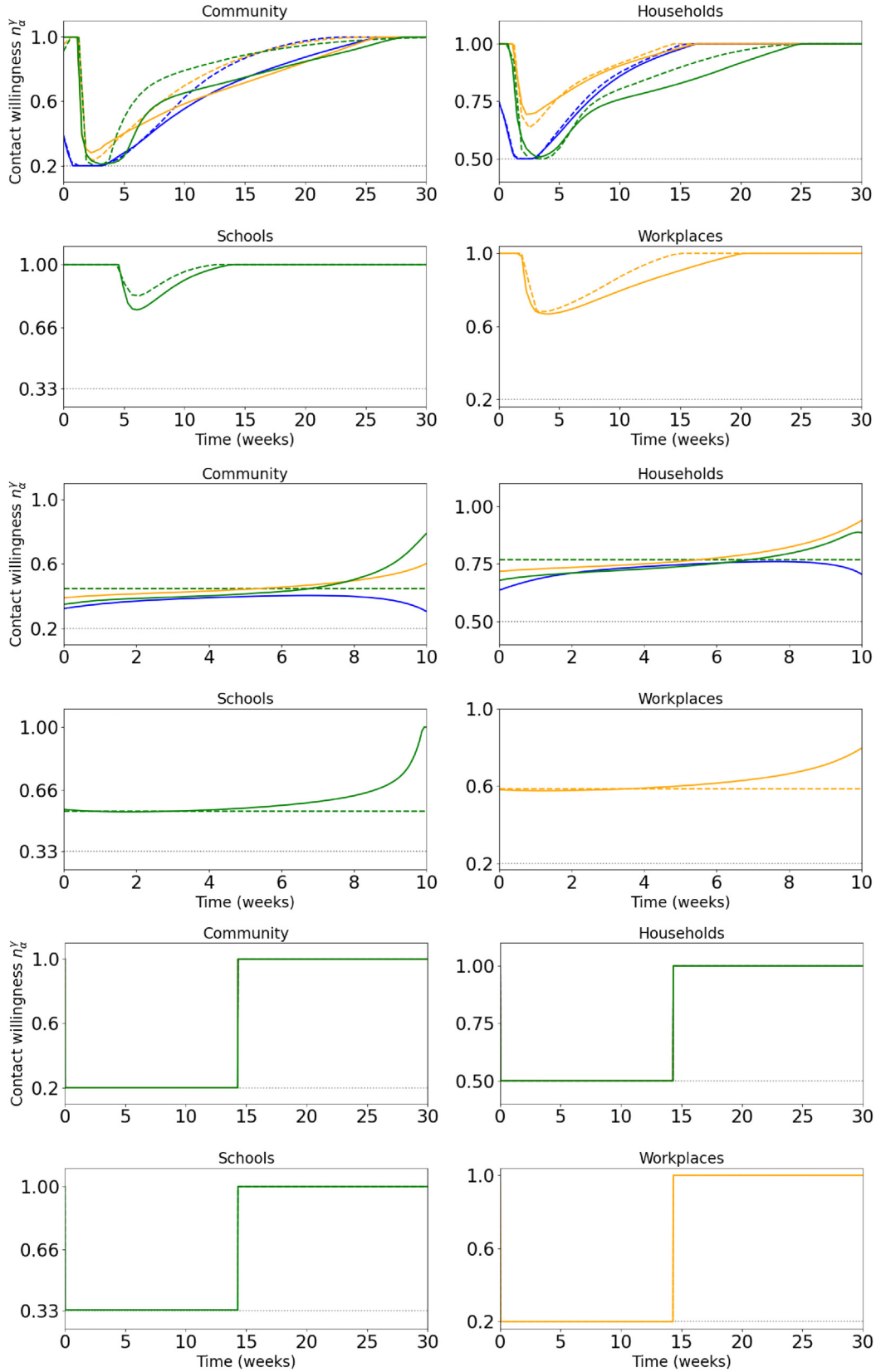


FIG. 14. Contacts willingness for the three template strategies defined in Sec. V (dotted lines) and the (finite- T) societal optimum for the corresponding parameters (solid lines). Rows 1 and 2: collective immunity ($T \rightarrow \infty$, computed in practice with $T = 100$ and $\tau_1 = 1$, dotted line) and societal optimum (computed with $T = 30$, $\tau_1 = 1$, $I_{\text{thr}} = 0$, solid line). Rows 3 and 4: contained strategy (dotted) and societal optimum (solid) for $T = 10$, $\tau_1 = 1$. Rows 5 and 6: eradication strategy (dotted) and societal optimum (solid) for $T = 30$, $\tau_1 = 1$, $I_{\text{thr}} = 1.10^{-5}$ —the two strategies match perfectly. Subpanels and legends are the same as in Fig. 7.

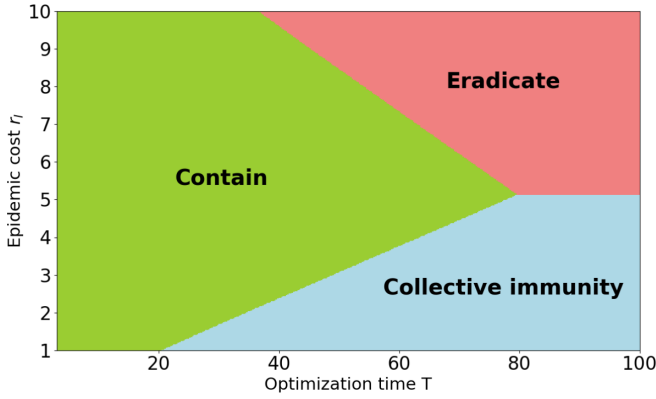


FIG. 15. Phase diagram showing the best type of strategy to follow among “reach collective immunity” (blue), “contain” (green), and “eradicate” (red) with the parameters of Tables II and III and $I_{thr} = 1.10^{-7}$ for the eradication strategy (it is more realistic, as it means $N_{tot} \simeq 10^7$). Change I_{thr} or the initial conditions will naturally change the transition lines (between immunity and eradication areas).

is small (below 20 weeks), the containment strategy is optimal whatever τ_1 . Then, there is a transient regime, where the optimal strategy can be any of the three scenarios, collective immunity, containment, or eradication according to τ_1 . Finally, after $T \simeq 80$ weeks, containing the epidemic is no longer an option, as the linear increase of the cost becomes prohibitive, and the best choice is either to reach collective immunity or to eradicate the epidemic. Since we use template strategies, the first-order phase transitions are represented by linear lines on the graph.

VI. CONCLUSION

In the present work we developed, following Ref. [38], an epidemic model based on the well-known SIR compartmental model supplemented by a social structure. This social structure relies on the idea that contacts are heterogeneous in society, both because individuals socialize in different contexts, and because they react in various ways to the disease (different perception of risk). Therefore, one can divide society into classes of agents which differ by their behavior, by the risk that the disease represents for them, and by the settings in which socialisation takes place. Here we used an age differentiation, but other kinds of classification (e.g., based on the immune status or on the presence of comorbidity) could easily be implemented within the same formalism. In the same way, one can easily add more compartments and more classes or settings to the model, without changing the global framework. The description of social structures obtained in this way is clearly less refined than one that would take into account the heterogeneity of social behaviors at an individual level, but it probably represents a good balance between precision and ease of application when trying to understand the dynamics of an epidemic and take appropriate, targeted action against it.

To this compartmental epidemic model with social structure, we have, following the approach of Turinici *et al.* [32], added a mean-field-game description of the dynamics: Agents may change their individual behavior depending whether they feel at risk of infection or not. After deriving the mean-field-game equations, we computed numerically the Nash

equilibrium, where each individual seeks to optimize his or her own interests. In this paradigm, individuals make a perfectly rational optimization, and are assumed to be able to performed the corresponding calculations which is something that we cannot expect from people in practice. The assumption here is thus rather than some central authority will solve the system (4.2)–(4.5) and provide to individuals their “best individual behavior” n_α^y which will be followed by agents if they sufficiently trust the institution.

As discussed in Sec. IV B, the choice of parameters we used for our simulations does not aim to describe a specific real-world configuration, but nevertheless corresponds to a rather generic situation, and the qualitative behavior we obtained is most likely rather typical of what would be observed in a realistic case. For this set of parameters, the Nash equilibrium obtained within the mean-field-game framework reduces significantly the costs associated with the epidemic when compared to the “business as usual” approach where social contacts are kept unchanged. However, there is usually still a gap between the MFG cost and the one that would correspond to the societal optimal policy, which represents the minimal global cost that can be borne by the society. To approach this optimal policy, we introduce the notion of “constrained Nash equilibrium,” in which we assume that under some conditions, the central authority can impose some constraints, analog to the partial lockdowns that we have seen during the COVID-19 epidemic, under simple rules which are known to the agents. In our work, we used a simple restrictive policy with three parameters ($\mathfrak{s}, \mathcal{J}_d, \mathcal{J}_1$) and we optimized this policy (i.e., we find the optimal set $[\mathfrak{s}^*, \mathcal{J}_d^*, \mathcal{J}_1^*]$) to get the lowest possible societal cost, and in this way close as much as possible the gap between the free Nash equilibrium and the societal optimum (see Figs. 8 and 11).

In our discussion of the Nash equilibrium and of the “constrained Nash” approach to the societal optimum, we have implicitly limited ourself to a regime of very long optimization time T , and of large population N_{tot} , for which the societal optimum policy necessary implies in some way to reach herd immunity. In Sec. V, we go back in more details to the analysis of the societal optimum, in particular lifting these constraints on T and N_{tot} . Depending (mainly) on the values of T , N_{tot} , and τ_1 , we can identify three *phases* that we label as “reach collective immunity” (the one implicitly assumed in the previous sections), “contain the epidemic” or “eradicate it” (see Fig. 15 showing which scenario is optimal depending on the parameters T and τ_1). The transition between any two of these phases can be understood as a first-order phase transition, in the sense that the associated strategies present discontinuities and are different from one phase to another. An important consequence of this discontinuity is that it is primordial for an authority to clearly identify the appropriate scenario, as a wrong choice could lead to significant additional costs.

Among these three scenarios, “reach collective immunity” is the one for which the time dependence of the agent strategies $\{n_\alpha^y(\cdot)\}$ are the more complex, and an authority will probably not be able to impose such exact strategy for all individuals. For this scenario, an approach through a mean-field-game paradigm under constraints as the one presented in this work is probably more relevant to approach the societal optimum cost, which would slightly shift the phases

boundaries in Fig. 15. However, the “containment strategy” appears to be easier to design for an authority, as it consists in adjusting in real time the constraints, depending on whether the epidemic is growing or not, to follow $R(t) \simeq 1$. Nevertheless, to find the best set of constraints to hold $R(t) \simeq 1$ still involves some complexity, as one should still adapt the strategy to the response of individuals. Advantage of this scenario is that this can be performed “on the fly,” and does not really imply any anticipation. Finally, in the “eradication strategy,” authority has to impose the maximum admissible constraints, which is conceptually rather simple. We stress, however, that, contrarily to the “herd immunity” strategy, the societal optimum obtained with strategy “contain” and “eradicate” are very far from any Nash equilibrium, even under “reasonable” constraints. The restrictions imposed with the two latter scenarios lead to epidemics which stay at low levels. In this context, the best individual strategy is to do essentially no effort, as there is almost no risk of infection. The social optimum strategy in this case is thus extremely far from the Nash equilibrium. This emphasizes a profound difference in nature between “herd immunity,” where individual optimization is closed to the societal optimum, and the two others where the gap is much more important. This would need to be considered by institutions when they will build collective strategies, as it is presumably very difficult to convince a population to follow on its own will a strategy which is far from a Nash equilibrium, and the required degree of coercion would significantly vary between the two cases.

The aim of this paper is to contribute to the construction of a theoretical framework on which authorities can rely to build appropriate policies against future epidemics. In particular, it showed that a relatively simple epidemic model including a differentiated behavior of rational agents can describe a number of different scenarios and is versatile to describe the outcome of various political choices. Our work emphasized both the challenge of this task and the extensive research which remains to be done. Indeed, our model still involves a number of parameters. While some of them (as the matrix \mathcal{M}) are known or could be relatively easily extracted from field data, some others (as τ_1 or the shape of f) are harder to apprehend, although they are crucial if one wants to use such type of models in an appropriate way. The model can be furthermore made more accurate with the addition of some extra cost such as the one associated with coordination in the case of restrictive policies. The question of evaluating quantities such as the risk induced by a possible epidemic is of course not specific to our model, and is actually one major task of epidemiologists. Here however we hope to provide a more formal framework from which possible course of action can be decided from that information.

From a theoretical perspective, further research could also be performed to improve the framework. First, one may want to integrate the spatio-temporal character of the dynamics taking into account heterogeneity of populations and regions around the world. Second, one could include, in the impact of constraints on individuals behavior, the feedback of the latter with respect to the imposed constraints. This is referred as Stackelberg games [59], which involve a set of agents (small players) and a principal player corresponding to authorities. This sort of games should reveal the importance of getting the

agreement of the population or not, depending of the choice of constraints. Third, we did not incorporate explicitly in our model the possible presence of a vaccine. Vaccination campaign also involve individuals behaviors and could be studied from a mean-field game point of view [29]. It can be added to the model but will rather concern another part of the epidemic, once vaccine is available, to optimize the vaccination campaign. A final active research domain is to infer accurately epidemic quantities with limited data sets, which it is almost always the case at the beginning of epidemics where limited number of tests are available.

Even without these improvements, the theoretical framework presented here should already be sufficiently flexible and realistic to be helpful in practice, as one could replace f or the generalized infection cost \mathcal{I}_α by the precise forms that would be obtained by field data, and then pursue the same analysis. We hope that authorities and institutions in charge of design policies against epidemics could use our work to improve accuracy of epidemics prediction as well as the efficiency of nonpharmaceutical interventions.

ACKNOWLEDGMENT

Louis Bremaud thanks the Centre for Quantum Technologies and the National University of Singapore for their hospitality.

APPENDIX A: DERIVATION OF THE SIR EQUATIONS

To prepare for the somewhat more involved discussion of Sec. II B, and to make the underlying hypotheses more explicit, we provide here a brief formal derivation of the SIR equations (2.1).

Let $x_k(t) \in \{s, i, r\}$ be the state of individual k at time t . The relative proportions of susceptible, infected, and recovered in a population of size N_{tot} can be written as

$$\begin{aligned} S(t) &= \frac{1}{N_{\text{tot}}} \sum_{k=1}^{N_{\text{tot}}} \delta_{x_k(t),s}, \\ I(t) &= \frac{1}{N_{\text{tot}}} \sum_{k=1}^{N_{\text{tot}}} \delta_{x_k(t),i}, \\ R(t) &= \frac{1}{N_{\text{tot}}} \sum_{k=1}^{N_{\text{tot}}} \delta_{x_k(t),r}, \end{aligned} \quad (\text{A1})$$

with $\delta_{a,b}$ as the Kronecker symbol.

Furthermore, an important property of the SIR model associated with the homogeneity of the population (all agents are connected with every other agent with a uniform probability) is that, in the $N_{\text{tot}} \rightarrow \infty$ limit, the system is *ergodic*, in the sense that averages over realizations of the Markov process and averages over individuals should correspond, i.e.,

$$(\forall k) \quad \lim_{N_{\text{tot}} \rightarrow \infty} \langle f_k \rangle = \lim_{N_{\text{tot}} \rightarrow \infty} \frac{1}{N_{\text{tot}}} \sum_{k'=1}^{N_{\text{tot}}} f_{k'} \quad (\text{A2})$$

(where $\langle f_k \rangle$ is the average over Markov realisations of the quantity f associated with a given individual k , and where the right-hand side is taken for an arbitrary (but single) real-

isation of this Markov process). Note that for this ergodicity to apply, not only N_{tot} should be large, but also the number of agents within each class and in particular the number of infected $N_{\text{tot}}I$, so that at the very beginning of the epidemic nonergodic behavior may exist if $I_0 < 1/N_{\text{tot}}$. In the $N_{\text{tot}} \rightarrow \infty$ limit that we consider here, however, we may and will write $(\langle S \rangle, \langle I \rangle, \langle R \rangle) = (S, I, R)$.

Let us consider an individual k which is susceptible at time t (i.e., $\delta_{x_k(t),s} = 1$). To become infected at time $t + dt$, this individual must meet an infected individual l in the time interval $[t, t + dt[$, and this encounter must lead to a transmission of the disease. Thus the proportion of individuals which are susceptible at time t and infected at time $t + dt$ is given, for a given realisation of the Markov process, by

$$S(t + dt) - S(t) = -\frac{1}{N_{\text{tot}}} \sum_{k=1}^{N_{\text{tot}}} \sum_{l=1}^{N_{\text{tot}}} C_{kl}(t) \delta_{x_k(t),s} \delta_{x_l(t),i}, \quad (\text{A3})$$

with $C_{kl}(t)$ the stochastic variable which take value 1 if k and l met during the interval $[t, t + dt[$ with a possible infection for k (if k is susceptible and l is infected), and 0 otherwise. This stochastic variable has an average value (over random realizations of the Markov process) which is the product of the probability of contact during dt , $\frac{1}{N_{\text{tot}}} \chi(t) dt$, by the transmission rate ρ since both events are independent. Note that since the population is assumed homogeneous, the probability of contact as well as the transmission rate are constant across the population (although the stochastic variables C_{kl} are not).

We then take the average over realizations assuming the independence of the three stochastic variables $\delta_{x_k(t),s}$, $\delta_{x_l(t),i}$, and C_{kl} , which amounts to assume that the events “individual k is susceptible at t ,” “individual l is infected at t ,” and “the pair of individuals (l, k) meet,” are independent because N_{tot} is large and the population is homogeneous. We get

$$\begin{aligned} \frac{d\langle S(t) \rangle}{dt} &= -\frac{1}{N_{\text{tot}}^2} \sum_{k=1}^{N_{\text{tot}}} \sum_{l=1}^{N_{\text{tot}}} \rho \chi(t) \langle \delta_{x_k(t),s} \rangle \langle \delta_{x_l(t),i} \rangle \\ &= -\rho \chi(t) \langle S(t) \rangle \langle I(t) \rangle. \end{aligned} \quad (\text{A4})$$

Using the identification between ensemble and population average, Eq. (A4) reduces to

$$\frac{dS(t)}{dt} = -\rho \chi(t) S(t) I(t). \quad (\text{A5})$$

The other SIR equations in Eq. (2.1) are obtained in the same way.

APPENDIX B: PARAMETERS OF THE MODEL

The values of the “social-structure” and “biological” parameters in Table II do not represent any particular real-life case, but are chosen to be representative of realistic situations, and therefore in the range typically found in the literature [1,38,47–50]. We take $\xi = 1.2 \text{ week}^{-1}$, not too far from the values $\xi = 7/6.5 = 1.1 \text{ week}^{-1}$ from Ref. [1], $\xi = 7/6.6 = 1.05 \text{ week}^{-1}$ from Ref. [50] and $\xi = 7/4 = 1.75 \text{ week}^{-1}$ from Ref. [47]. The contagiousness ρ is assumed to be 0.1, similar to the value mentioned in Ref. [47] for the COVID-19, where it is slightly lower (about 0.08). Regarding μ , we choose $\mu = 0.2$, of the same order of magnitude as in Ref. [50]. Similarly, for the proportion of individuals in the population, the distribution

(25%, 50%, 25%) is closed to the one in Ref. [50], where it is 22% if you gather the proportion of children and teenagers, 57% for adults, and 21% for seniors. The contact matrices $\mathcal{M}_{\alpha\beta}^{\gamma}$ are inspired by Ref. [38] for their shape: Almost all contacts in schools are between children, an similarly inside workplaces for adults. In the community, all individuals have the same probability of meeting other individuals, while in households the structure is a bit more complex, with a strong child-adult link and senior-senior contacts. The absolute value of contacts is then normalized so that the average total number of contacts is close to the values presented in Ref. [47]. Finally, to ensure the consistency of our choices, we check that all these collected quantities give a reproductive number $\tilde{R}_0 = 2.9$ with the method described in Refs. [38,60] for calculating \tilde{R}_0 at the beginning of epidemics in heterogeneous populations. This value is consistent with the literature for viruses such as COVID-19 [13]. The choice of initial conditions ($I_{\alpha}(t=0)$) is taken uniform among age classes, and since we do not consider stochastic effects at the beginning of epidemics, we take a value of 1% which has little effect on the simulation as long as it is small enough.

APPENDIX C: ARBITRARY ASYMPTOMATICITY

In this Appendix, we generalize the discussion of Sec. III A to arbitrary values of the asymptomaticity parameter $\mu \in [0, 1]$. In that case the equations change only slightly. As before, only asymptomatic infected individuals participate to the propagation of the disease. Asymptomatic individuals ignore their status, and if infected feel no harm; as a consequence, they will not change their behavior upon contamination at time τ (thus the integral in Eq. (3.1) will extend up to T), nor bear the health costs [thus the second term in Eq. (3.1) will be zero for them]. The cost for asymptomatic individuals thus reads

$$C_a(n_a^{\gamma}(\cdot), \{n_b^{\gamma}(\cdot)\}, t, \tau) \equiv \int_t^T f_a(n_a^{\gamma}(t')) dt'. \quad (\text{C1})$$

Since the agent ignores whether she is asymptomatic or not, the average cost she anticipates is with probability $(1 - \mu)$ the estimated cost (3.9) and with probability μ the cost (C1) (which is independent of τ); therefore,

$$\begin{aligned} \mathcal{C}_a^{\mu}(n_a^{\gamma}(\cdot), t) &= (1 - \mu) \int_t^T (f_a(n_a^{\gamma}(t')) + \lambda_a(t') \mathcal{I}_{\alpha}(I(t'))) \\ &\quad \times (1 - \phi_a(t')) dt' + \mu \int_t^T f_a(n_a^{\gamma}(t')) dt' \\ &= \int_t^T [(1 - \mu) \lambda_a(t') \mathcal{I}_{\alpha}(I(t')) (1 - \phi_a(t')) \\ &\quad + f_a(n_a^{\gamma}(t')) (1 - (1 - \mu) \phi_a(t'))] dt'. \end{aligned} \quad (\text{C2})$$

The term $(1 - \mu) \phi_a(t')$ can be interpreted as the probability for an individual of age class α to be infected and symptomatic before t' , since the two events “have been infected before t' ” and “be symptomatic” are independent. In the limit of $\mu \ll 1$, we recover the cost derived before in Eq. (3.9); note that to allow an epidemic growth in this limit we assume that $\mu \rho$ and thus λ_a are of the same order in μ as ξ (the recovery rate), that is, of order 0 in μ .

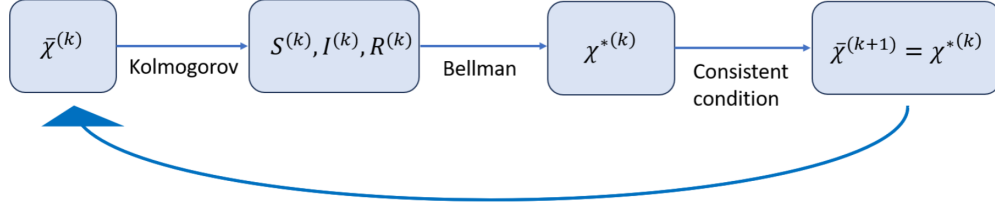


FIG. 16. Global scheme used for the inductive sequence.

APPENDIX D: NUMERICAL IMPLEMENTATION

1. Numerical resolution of the Nash equilibrium

We describe here two numerical methods we have implemented to reach the Nash equilibrium: an inductive sequence method and a gradient descent. Again, we omit the superscript γ to lighten the notations.

a. First method: Inductive sequence

The first method is the most natural one. The idea is the following. We start with an initial global strategy $n_\alpha^{(0)}(\cdot)$ (the brackets (\cdot) indicate that this initial strategy is given at all times), and we compute the associated epidemic quantities $(S^{(0)}(\cdot), I^{(0)}(\cdot), R^{(0)}(\cdot))$ with Eq. (4.2) for these given initial conditions. Then, using Eq. (4.9), we compute the best individual response to this epidemics dynamics, $n_\alpha^{*(0)}$. Since the latter should be followed by all individuals, we obtain a new global strategy $n_\alpha^{(1)} = n_\alpha^{*(0)}$. We repeat the process until we reach the Nash equilibrium condition $n_\alpha^{(k)} \simeq n_\alpha^{*(k)}$ for a sufficiently large k .

To summarize, the global scheme of this method is the following, performed simultaneously for all age classes α : Each step is quite straightforward numerically since we only deal with classical partial differential equations. Figure 16 corresponds to an inductive sequence $n_\alpha^{(k+1)} = F(n_\alpha^{(k)})$ where the functional F is defined as $F(n_\alpha^{(k)}) = n_\alpha^{*(k)}$. However, this inductive sequence will not always converge to a fixed point of F , which is why we consider a second approach below.

In practice, we discretized the interval $[0, T]$ with $T = 40$ weeks using ~ 150 time steps; typically the number of iterations to reach the fixed points is ~ 10 .

b. Second method: Gradient descent

To deal with cases where the inductive sequence does not converge, we use a gradient descent on the variable $n_\alpha(\cdot)$ of the cost \mathfrak{C}_a [see Eq. (3.9)] to reach the Nash equilibrium. We use the following scheme for each age class α with representative individual a

$$n_a^{(k+1)}(t) = n_a^{(k)}(t) - h \cdot \nabla_1 \mathfrak{C}_a(n_a^{(k)}(\cdot), \{n_\beta^{(k)}(\cdot), t\}) \Big|_{n_a^{(k)}(\cdot) = n_a^{(k)}(\cdot)}, \quad (\text{D1})$$

where ∇_1 means that the gradient is taken on $n_a^{(k)}(\cdot)$. The dot in Eq. (D1) indicates a scalar product, h and ∇_1 are vectors indexed by γ . This scheme gives $\nabla_1 \mathfrak{C}_a(n_a^{(k)}(\cdot), \{n_\beta^{(k)}(\cdot), t\}) = 0$ when we reach the equilibrium. That is, we are at a local minimum of the cost \mathfrak{C}_a with respect to the first variable $n_a(\cdot)$. We can then check numerically that we are indeed at the true Nash equilibrium, that is, at a global minimum for the variable

$n_\alpha(\cdot)$ (for each age class α), by checking that $F(n_{\text{Nash}}) = n_{\text{Nash}}$ for a given Nash candidate n_{Nash} .

To make the numerical computation of the gradient $\nabla_1 \mathfrak{C}_a$ less heavy and more efficient, we first perform a few analytical steps. To avoid heavy notations, the cost at $t = 0$ will be denoted as $\mathfrak{C}_a(n_a, n_\beta)$. We have

$$\begin{aligned} \mathfrak{C}_a(n_a, n_\beta) &\equiv \mathfrak{C}_a(n_a^\gamma(\cdot), \{n_\beta^\gamma(\cdot)\}, 0) \\ &= \int_0^T (f_\alpha(n_a^\gamma(s)) + \lambda_\alpha(s) \mathcal{I}_\alpha(I(s))) (1 - \phi_\alpha(s)) ds. \end{aligned} \quad (\text{D2})$$

To compute the gradient of the cost with respect to the first variable, we introduce the functional derivative of \mathfrak{C}_a with respect to its first variable n_a , in the direction h (with h a function, usually a Dirac delta). By definition,

$$D_h \mathfrak{C}_a(n_a, n_\beta) \equiv \lim_{\epsilon \rightarrow 0} \frac{1}{\epsilon} (\mathfrak{C}_a(n_a + \epsilon h, n_\beta) - \mathfrak{C}_a(n_a, n_\beta)). \quad (\text{D3})$$

Using the definition of the gradient, this functional derivative can be reexpressed as

$$D_h \mathfrak{C}_a(n_a, n_\beta) = \int_0^T h(t) \cdot \nabla_1 \mathfrak{C}_a(n_a, n_\beta, t) dt. \quad (\text{D4})$$

which explicitly written gives $h(t) \cdot \nabla_1 \mathfrak{C}_a = \sum_\gamma h^\gamma(t) \frac{\delta \mathfrak{C}_a}{\delta n_a^\gamma(t)}$ with $\frac{\delta \mathfrak{C}_a}{\delta n_a^\gamma(t)}$ the functional derivative of the total cost \mathfrak{C}_a with respect to $n_a^\gamma(t)$. Since $1 - \phi_\alpha(s) = \exp(-\int_0^s \lambda_\alpha(u) du)$, the cost (D2) depends on n_a through the terms $f_\alpha(n_a)$ and λ_α via (3.6); with λ_α is linear in n_a . Using Eq. (D3) we have at first order $\lambda_\alpha(n_a + \epsilon h) = \lambda_\alpha(n_a) + \epsilon h \cdot \frac{d\lambda_\alpha}{dn_a}(t)$ with $\frac{d\lambda_\alpha}{dn_a}(t)$ a vector indexed by γ , of components

$$\frac{d\lambda_\alpha}{dn_a^\gamma}(t) \equiv \mu \rho \sum_{\beta=1}^{n_{\text{cl}}} n_\beta^\gamma(t) \mathcal{M}_{\alpha\beta}^{\gamma(0)} I_\beta(t). \quad (\text{D5})$$

We then use the integral form (D2) to expand Eq. (D3) to lowest order in ϵ . One of the terms involves a double integral; to put $D_h \mathfrak{C}_a(n_a, n_\beta)$ under the form (D4), we invert integrands and change variables, namely $\int_0^T [f(t) \int_0^t g(s) ds] dt = \int_0^T [g(t) \int_t^T f(s) ds] dt$. Once the expression is of the form (D4) we can read off the value of the gradient $\nabla_1 \mathfrak{C}_a(n_a, n_\beta)$:

$$\begin{aligned} \nabla_1 \mathfrak{C}_a(n_a, n_\beta, t) &= \left[\frac{df_\alpha}{dn_a}(n_a(t)) + \frac{d\lambda_\alpha}{dn_a}(t) \mathcal{I}_\alpha(I(t)) \right] (1 - \phi_\alpha(t)) \\ &\quad - \frac{d\lambda_\alpha}{dn_a}(t) \int_t^T (f_\alpha(n_a(s)) + \lambda_\alpha(s) \mathcal{I}_\alpha(I(s))) \\ &\quad \times (1 - \phi_\alpha(s)) ds, \end{aligned} \quad (\text{D6})$$

with $\frac{df_\alpha}{dn_\alpha}$ the derivative of f_α with respect to the variable $n_\alpha^\gamma(t)$ (with a vector notation). The straight d used here indicates usual derivatives, as f and λ are functions (and not functional) of $n_\alpha^\gamma(t)$. The gradient (D6) is then computed numerically to follow the scheme (D1).

2. Numerical resolution of the constrained Nash equilibrium

For the constrained Nash equilibrium, the strategies $n_\alpha^k(t)$ in Eq. (D1) additionally must fulfill constraints such as Eq. (4.11). Since these constraints are active or not depending on the value of $I(t)$, at each step k one must check that the strategies respect the constraints defined by the values of the epidemic rate at step k . Each step of the gradient descent therefore comprises two parts. In the first part, we perform the same gradient descent as the one described for the Nash equilibrium Appendix D 1 b, but now we check that the new strategies $\{n_\alpha^{k+1}(\cdot)\}$ respect the constraints defined by the $I(\cdot)$ from step k ; if they do not, we enforce them by correcting accordingly the $\{n_\alpha^{k+1}(\cdot)\}$. In the second part, we compute the new epidemic rates and find the corresponding new constraints.

An issue appears when we approach the Nash equilibrium. The variation of the constraints and of the strategy $\{n_\alpha^{k+1}(\cdot)\}$ can form some cycles which impede convergence. To bypass this difficulty, we choose to freeze the constraints at some step k and continue the gradient descent process as in the method Appendix D 1 b; after some steps, we recompute the constraints and we continue the process until the convergence.

3. Numerical resolution of the societal optimum

We can reach the optimal strategy through different ways. Here we choose to make a gradient descent on the cost $\mathcal{C}_{\text{glob}}$, but one can also use the Pontryagin maximum principle [51]. We optimize the behavior of individuals to minimize the total cost paid by the population

$$\mathcal{C}_{\text{glob}}(\{n_\beta^\gamma(\cdot)\}) = \sum_\alpha \mathcal{N}_\alpha \mathcal{C}_\alpha(\{n_\beta(\cdot)\}), \quad (\text{D7})$$

where the cost depends on all the functional $\{n_\beta^\gamma\}$ in an equal footing. For simplicity, we will denote this global strategy over all classes and setting n . To do this minimization, we will follow the same scheme as described in Eq. (D1). We thus have to compute $\nabla \mathcal{C}_{\text{glob}}(n, t)$, which only involves all the collective strategies n and the time t at which the gradient is evaluated. For each age class α , we calculate the gradient

$$D_h \mathcal{C}_\alpha(n) \equiv \int_0^T h(t) \cdot \nabla \mathcal{C}_\alpha(n, t) dt, \quad (\text{D8})$$

to identify $\nabla \mathcal{C}_\alpha(n, t)$ as in Appendix D 1 b, with ∇ is now on the global strategy n and having components along γ and β (as does h). New terms appear because quantities such as the proportion of infected individuals $I(\cdot)$ now depend on all n_β . Below, we outline the key steps involved in the calculation. The first step is deriving the functional derivative of the gradient $D_h \mathcal{C}_\alpha(n, t)$. Starting from the expression of \mathcal{C}_α in Eq. (3.9),

we get

$$\begin{aligned} D_h \mathcal{C}_\alpha(n_\beta, t) \\ = D_h \left[\int_t^T (f_\alpha(n_\alpha(s)) + \lambda_\alpha(s) \mathcal{I}_\alpha(I(s))) (1 - \phi_\alpha(s)) ds \right]. \end{aligned} \quad (\text{D9})$$

Thus, we need to compute each functional derivative of the terms appearing in Eq. (D9), which gives

$$\begin{aligned} D_h \lambda_\alpha(t) = \lim_{\epsilon \rightarrow 0} \frac{1}{\epsilon} \left[\sum_\gamma \sum_\beta \rho \mathcal{M}_{\alpha\beta}^\gamma (n_\alpha^\gamma(t) + \epsilon h_\alpha^\gamma(t)) (n_\beta^\gamma(t) \right. \\ \left. + \epsilon h_\beta^\gamma(t)) (I_\beta(t) + \epsilon D_h I_\beta(t)) \right], \end{aligned} \quad (\text{D10})$$

$$D_h \phi_\alpha(t) = (1 - \phi_\alpha(t)) \int_0^t D_h \lambda_\alpha(s) ds, \quad (\text{D11})$$

$$D_h I_\beta(t) = \int_0^t \frac{\delta I_\beta(t)}{\delta n(s)} \cdot h(s) ds, \quad (\text{D12})$$

$$D_h f_\alpha(n_\alpha(t)) = d_n f_\alpha(n_\alpha(t)) \cdot h(t), \quad (\text{D13})$$

$$D_h \mathcal{I}_\alpha(I(t)) = \frac{\kappa_\alpha \mathbf{r}_1 q_{\text{sat}}}{\mathcal{J}_{\text{sat}}} D_h I(t) \exp \left[q_{\text{sat}} \frac{I(t) - \mathcal{J}_{\text{sat}}}{\mathcal{J}_{\text{sat}}} \right], \quad (\text{D14})$$

where the dots in Eqs. (D10), (D12), and (D13) indicate that h and n are indexed by β and γ and indices are summed over. In Eq. (D12), $\delta I_\beta(t)/\delta n(s)$ indicates the functional derivative of $I_\beta(t)$ with respect to the collective behavior $n(s)$. This “time delayed” derivative is the crucial term of the gradient for the societal optimum, one can perform a linearization of Eqs. (2.12) to propagate linearly the elementary deformation of I_β from time s to time t to avoid several numerical computation of the whole epidemic. As in Appendix D 1 above, we use these expressions to compute explicitly Eq. (D9) and put it under the form Eq. (D8), which gives the expression of $\nabla \mathcal{C}_\alpha(n, t)$. We can then perform the gradient descent scheme Eq. (D1) numerically and efficiently without several computations of the whole epidemic at each time t .

APPENDIX E: COMPARISON OF GLOBAL COST FOR THE NASH EQUILIBRIUM UNDER DIFFERENT CONSTRAINTS

In this Appendix, we study how the global cost for the Nash equilibrium under constraints changes with the three parameters of the constraint; results are displayed in Fig. 17. The parameters used in Fig. 8 correspond to the minimum found here.

At $\mathfrak{s} = 0$ we recover the free Nash equilibrium, with the same global cost, around $C_{\text{glob}} = 120$. When the intensity \mathfrak{s} is increased, society carries a lower cost than in the free Nash equilibrium, because all individuals are forced to make some efforts. But at a certain intensity, a minimum is reached; the location of this minimum is mainly influenced by \mathbf{r}_1 , and corresponds here to the region around $\mathfrak{s} = 0.3\text{--}0.4$. In this interval, we find the optimal lockdown configuration that we presented above with $\mathfrak{s} = 0.35$, $\mathcal{J}_d = 0.12$, $\mathcal{J}_1 = 4.10^{-4}$. Among the three parameters (\mathfrak{s} , \mathcal{J}_d , \mathcal{J}_1) characterizing the partial lockdown, the one which has the most impact on the global cost is \mathfrak{s} , as there are no significant variations between the

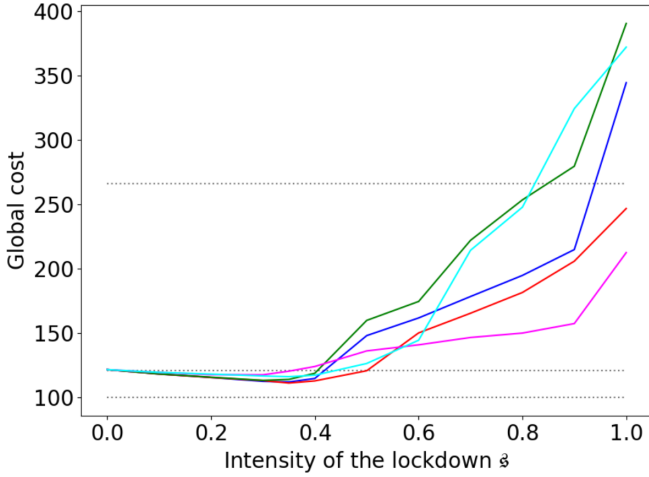


FIG. 17. Comparison of global cost for different parameters of the constraints. The x axis corresponds to the intensity of the lockdown s , which could vary from 0 (no constraints) to 1 (maximal constraints). The different curves correspond to different choices for the two threshold parameters \mathcal{J}_d and \mathcal{J}_1 . We choose $\mathcal{J}_d = (0.12, 0.08, 0.04)$, a too low \mathcal{J}_d will clearly deteriorate the situation as it will impose a duration of the constraints which is too long to reach collective immunity. A higher \mathcal{J}_d is, however, not effective, as typically the maximum effort with the free Nash equilibrium is around 0.15 for our choice of parameters, and thus the threshold would never be reached. For \mathcal{J}_1 we took $\mathcal{J}_1 = (1.10^{-2}, 4.10^{-4}, 1.10^{-5})$. \mathcal{J}_1 will have a major impact on the duration Δt of constraints, with a log relation of the form $\Delta t \simeq -\log(\mathcal{J}_1)$. Increasing \mathcal{J}_1 will decrease the extent of lockdowns and conversely. A too high \mathcal{J}_1 will lead to epidemic rebounds (the constraints is lifted too early), and a too low \mathcal{J}_1 will impose useless extra social cost to the population. Blue curve $(\mathcal{J}_d, \mathcal{J}_1) = (0.08, 4.10^{-4})$, red $(0.12, 4.10^{-4})$, green $(0.04, 4.10^{-4})$, magenta $(0.08, 1.10^{-2})$, and cyan $(0.08, 1.10^{-5})$. Dotted gray horizontal lines from top to bottom correspond, respectively, to business as usual cost, free Nash equilibrium, and societal optimum.

different curves of Fig. 17. For $s > 0.5$, the constraints become too strong with respect to the epidemic threat for all choices of thresholds, but especially for low \mathcal{J}_d and \mathcal{J}_1 , because this imposes long constraints which become very costly as s increases. When s approaches 1 we even reach a point above the business as usual scenario (which had $C_{\text{glob}} = 266$), as we enter a regime characterized by a succession of lockdowns followed by epidemic rebounds which are suppressed by the next lockdown before herd immunity can be reached.

APPENDIX F: ERADICATION STRATEGY

In this Appendix, we show that the optimal eradication strategy is to hold the maximum amount of efforts in the interval $[0, t_{\text{thr}}]$ until the eradication of the epidemic when $I(t_{\text{thr}}) = I_{\text{thr}}$, and then completely release the efforts. This strategy is sometimes referred in the literature as a bang-bang strategy [35]. To show that this strategy is optimal, we have to show that any small reduction of efforts δn made during δt in the interval $[0, t_{\text{thr}}]$ will increase t_{thr} so that the total cost paid by individuals will be higher. Without loss of generality, we consider that time 0 corresponds to the time at which we

start the efforts. We refer to this slightly different strategy as the deviating strategy, and the associated epidemic is denoted \tilde{I} . However, t_{thr} will increase by a time $\delta\tau$, as the time at which epidemic vanishes will be greater. We are left with a competition between two costs: $d_n f(n_{\text{min}}) \delta t \delta n$ which is the (negative) cost caused by the reduction of efforts (this is a gain from the individual point of view), and $\delta\tau f(n_{\text{min}})$ which is the extra (positive) cost that individuals will pay to eradicate the epidemic. To compare these costs, we need to evaluate $\delta\tau$ in terms of δt and δn .

At t_{thr} , one has $I(t_{\text{thr}}) = 0$. For the deviating strategy, one has $\tilde{I}(t_{\text{thr}} + \delta\tau) = 0$, where $\tilde{I}(t) \equiv I(t) + \delta I(t)$, with $\delta I(t)$ the small difference amount of infected between the two strategies. We get

$$\begin{aligned} (I + \delta I)(t_{\text{thr}} + \delta\tau) &= I(t_{\text{thr}}), \\ \dot{I}(t_{\text{thr}}) \delta\tau + \delta I(t_{\text{thr}}) &= 0, \\ \delta\tau &= -\frac{\delta I(t_{\text{thr}})}{\dot{I}(t_{\text{thr}})}, \end{aligned} \quad (\text{F1})$$

which allows us to evaluate $\delta\tau$. Indeed, at time t_{thr} we have $\dot{I}(t_{\text{thr}}) \simeq -\xi I_{\text{thr}}$, as the number of new infected is completely negligible at this point. *A priori*, since there is a little spread of the epidemic in the population we will have $\delta I(t_{\text{thr}}) > \delta I(0) \exp(-\xi t_{\text{thr}})$, and close to this value if $I(0)$ is small enough. Therefore, we get $\delta\tau > \frac{\delta I(0)}{\xi I_{\text{thr}}} \exp(-\xi t_{\text{thr}})$. At this stage, we need to give an order of magnitude for t_{thr} . We use that $I(t_{\text{thr}}) \simeq I(0) \exp(-\xi t_{\text{thr}}) = I_{\text{thr}}$ and thus $\delta\tau > \frac{\delta I(0)}{\xi I(0)}$. One can then easily show that $\delta I(0) \propto \delta n \delta t$ where the proportionality coefficient can be written in a formal way as $\frac{\partial \lambda}{\partial n}(n_{\text{min}}) S(0)$ where we omit age class notations (generalization is straightforward). Finally, we get the extra cost δC paid by individuals,

$$\begin{aligned} \delta C &= d_n f(n_{\text{min}}) \delta t \delta n + \delta\tau f(n_{\text{min}}) \\ &> \delta t \delta n \left[d_n f(n_{\text{min}}) + f(n_{\text{min}}) \frac{\partial \lambda}{\partial n}(n_{\text{min}}) S(0) \right] > 0. \end{aligned} \quad (\text{F2})$$

For any positive $\delta t, \delta n$, one can check that $[d_n f(n_{\text{min}}) + f(n_{\text{min}}) \frac{\partial \lambda}{\partial n}(n_{\text{min}}) S(0)] > 0$, where $\frac{\partial \lambda}{\partial n} \propto I(0)$ with $I(0) \geq I_{\text{thr}}$. The extra cost paid by individuals for the deviating strategy is always positive, it is therefore worse than the initial one. The initial strategy presented at the beginning of this Appendix is the optimal one in this sense. One can also argue that this local minimum is the true minimum among all eradicating strategies, as the above reasoning will be *a priori* true for higher values of n , considering the shape of f .

APPENDIX G: EXPLORATION OF THE PARAMETER SPACE

We present below the Nash equilibrium results (first for epidemic quantities in Fig. 18 and then for contact willingness in Fig. 19) where we change at each time one of the parameters presented in Tables II and III. We see in Fig. 18 that the general behaviors observed with the original set of parameters (unicity of the peak, reach collective immunity) are quite robust to many different changes. As expected, contacts between classes allow an epidemic spreading even in classes where no one is infected at $t = 0$ (first row). Then,

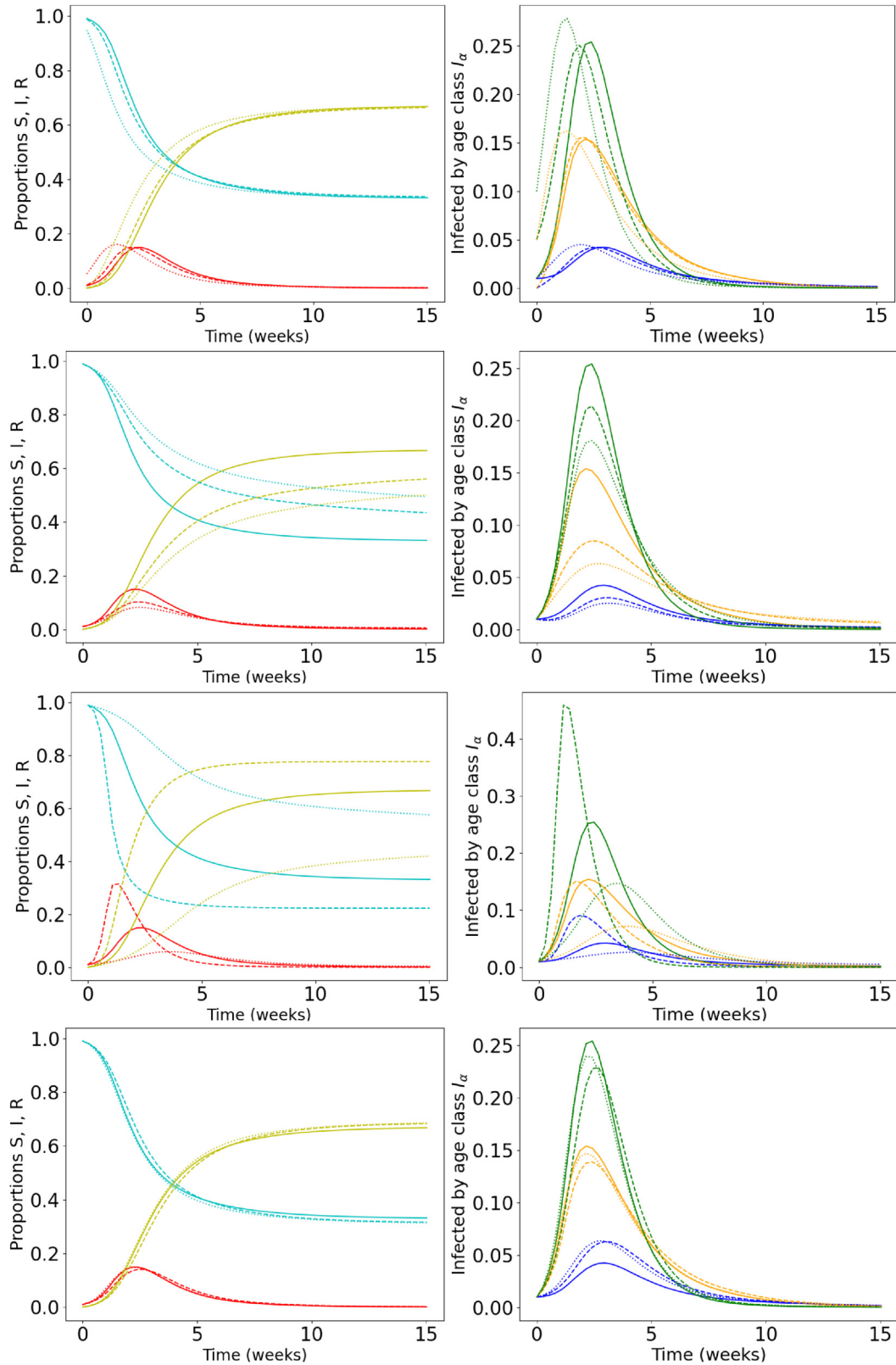


FIG. 18. Comparison of Nash equilibrium epidemics for the set of parameters of Tables II and III with one (arbitrary but realistic) parameter change for each row (solid lines correspond to baseline parameters). Color legend is the same as in Fig. 6. First row: initial conditions change with $(S_0(0), S_1(0), S_2(0)) = (0.99, 0.99, 0.99)$ for solid line, dashed (0.95, 1, 1) and dotted (0.9, 0.95, 0.99). In each case, $I_\alpha(0) = 1 - S_\alpha(0)$ and $R_\alpha(0) = 0$. Second row: three different τ_1 with $\tau_1 = 1$ (solid), $\tau_1 = 3$ (dashed), and $\tau_1 = 5$ (dotted). Third row: three different proportions in the population, $(\mathcal{N}_0, \mathcal{N}_1, \mathcal{N}_2) = (0.25, 0.5, 0.25)$ for solid line, (0.6, 0.2, 0.2) for dashed lines, and (0.2, 0.2, 0.6) for dotted lines. Fourth row: three different matrices \mathcal{M}_1 (solid), \mathcal{M}_2 (dashed), and \mathcal{M}_3 (dotted) defined in Table IV.

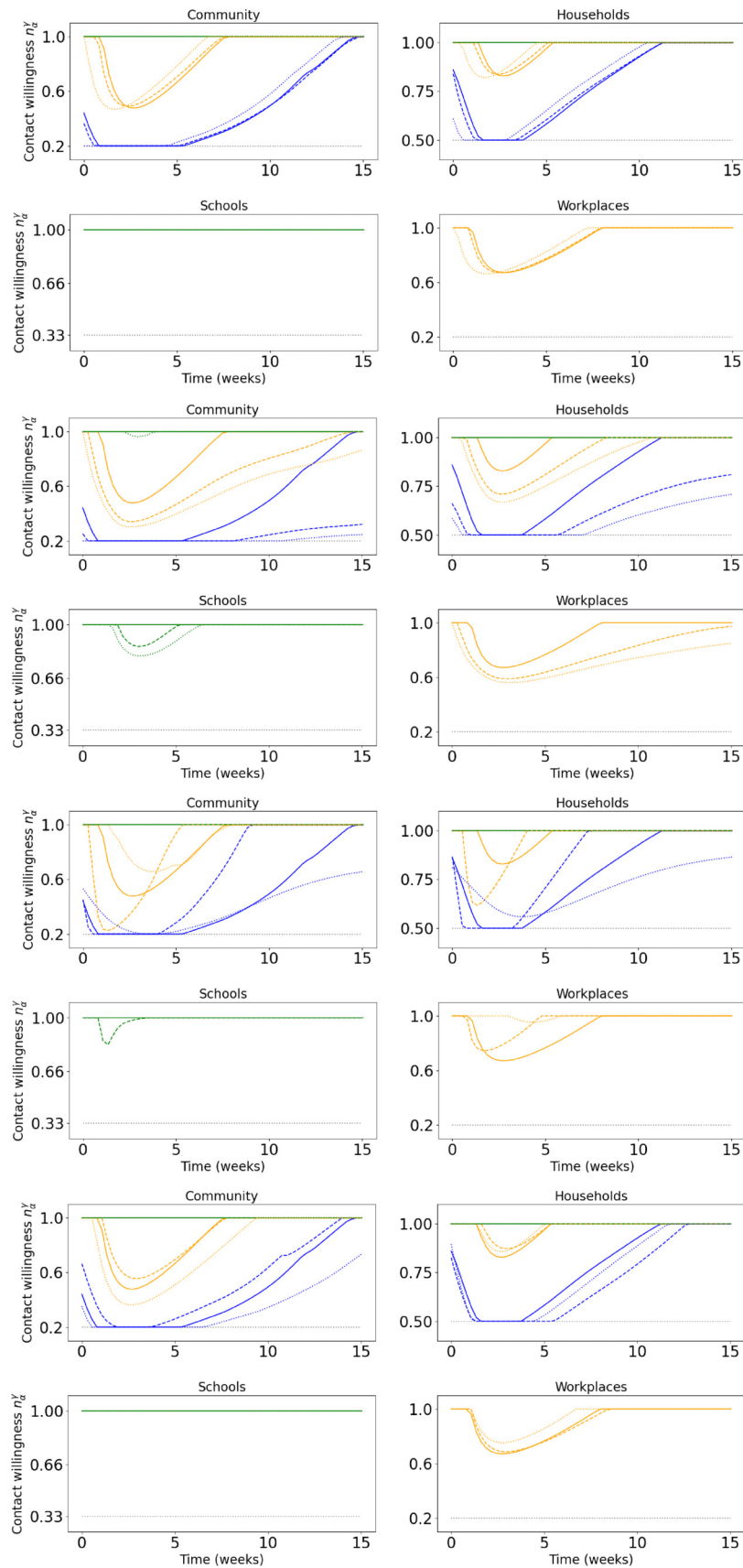


FIG. 19. Comparison of Nash equilibrium contact willingness for the different set of parameters used in Fig. 18 and the same legend for solid, dashed, and dotted lines. We keep the legend of Fig. 7 regarding colors.

TABLE IV. Table of matrices \mathcal{M}_1 , \mathcal{M}_2 , and \mathcal{M}_3 (given with the form \mathcal{M}^{ν}) used for the fourth row of Fig. 18. The first one corresponds to the one we took in our previous simulations (Tables II and III), while the two others are chosen to explore two behaviors: Matrix \mathcal{M}_2 corresponds to a society with important heterogeneous contacts, especially in households; while matrix \mathcal{M}_3 is a society which is more homogeneous with a lot of contacts in community. Matrix elements are contact rates (per week) in our model.

\mathcal{M}_1^S	\mathcal{M}_1^W	\mathcal{M}_1^C	\mathcal{M}_1^H
$\begin{pmatrix} 100 & 0 & 0 \\ 0 & 0 & 0 \\ 0 & 0 & 0 \end{pmatrix}$	$\begin{pmatrix} 0 & 0 & 0 \\ 0 & 75 & 0 \\ 0 & 0 & 0 \end{pmatrix}$	$\begin{pmatrix} 12.5 & 25 & 12.5 \\ 12.5 & 25 & 12.5 \\ 12.5 & 25 & 12.5 \end{pmatrix}$	$\begin{pmatrix} 15 & 25 & 10 \\ 12.5 & 32.5 & 5 \\ 10 & 10 & 30 \end{pmatrix}$
\mathcal{M}_2^S	\mathcal{M}_2^W	\mathcal{M}_2^C	\mathcal{M}_2^H
$\begin{pmatrix} 100 & 0 & 0 \\ 0 & 0 & 0 \\ 0 & 0 & 0 \end{pmatrix}$	$\begin{pmatrix} 0 & 0 & 0 \\ 0 & 75 & 0 \\ 0 & 0 & 0 \end{pmatrix}$	$\begin{pmatrix} 12.5 & 15 & 5 \\ 7.5 & 25 & 5 \\ 5 & 10 & 12.5 \end{pmatrix}$	$\begin{pmatrix} 12.5 & 15 & 20 \\ 7.5 & 30 & 17.5 \\ 20 & 35 & 12.5 \end{pmatrix}$
\mathcal{M}_3^S	\mathcal{M}_3^W	\mathcal{M}_3^C	\mathcal{M}_3^H
$\begin{pmatrix} 75 & 0 & 0 \\ 0 & 0 & 0 \\ 0 & 0 & 0 \end{pmatrix}$	$\begin{pmatrix} 0 & 0 & 0 \\ 0 & 50 & 0 \\ 0 & 0 & 0 \end{pmatrix}$	$\begin{pmatrix} 25 & 50 & 25 \\ 25 & 50 & 25 \\ 25 & 50 & 25 \end{pmatrix}$	$\begin{pmatrix} 12.5 & 25 & 12.5 \\ 12.5 & 25 & 12.5 \\ 12.5 & 25 & 12.5 \end{pmatrix}$

in second row regarding different τ_1 , we see that epidemic peak occurs at a lower level as τ_1 increases, since individuals do more efforts to protect themselves. In third row, we see that the different proportion of age classes in the population will have a huge impact on the epidemic. Indeed, it will affect both the matrix of effective contacts (which are higher between young people) and the risk due to infection (which

is lower for young). Hence, the observed behavior results in a high and quick epidemic for a young population, while it is significantly lower and slower for an old population. Finally, in the fourth row, the precise matrix of contacts \mathcal{M} affects the epidemic in each class, but in a relatively moderate way regarding the global evolution of infected proportion in the population.

- [1] N. Ferguson, D. Laydon, G. Nedjati Gilani, N. Imai, K. Ainslie, M. Baguelin, S. Bhatia, A. Boonyasiri, Z. Cucunuba Perez, G. Cuomo-Dannenburg *et al.*, Report 9: Impact of non-pharmaceutical interventions (NPIs) to reduce COVID-19 mortality and healthcare demand, *Technical Report* (Imperial College, London, UK, 2020).
- [2] D. K. Miles, M. Stedman, and A. H. Heald, “Stay at Home, Protect the National Health Service, Save Lives”: A cost benefit analysis of the lockdown in the United Kingdom, *Int. J. Clin. Pract.* **75**, e13674 (2021).
- [3] A. A. Toda, Susceptible-infected-recovered (SIR) dynamics of COVID-19 and economic impact, [arXiv:2003.11221](https://arxiv.org/abs/2003.11221).
- [4] J. D. Osofsky, H. J. Osofsky, and L. Y. Mamon, Psychological and social impact of COVID-19, *Psychol. Trauma: Theory, Res., Practice, Policy* **12**, 468 (2020).
- [5] Q. D. Nguyen and M. Prokopenko, A general framework for optimising cost-effectiveness of pandemic response under partial intervention measures, *Sci. Rep.* **12**, 19482 (2022).
- [6] R. Morton and K. H. Wickwire, On the optimal control of a deterministic epidemic, *Adv. Appl. Probab.* **6**, 622 (1974).
- [7] K. H. Wickwire, Optimal isolation policies for deterministic and stochastic epidemics, *Math. Biosci.* **26**, 325 (1975).
- [8] F. D. Sahneh, F. N. Chowdhury, and C. M. Scoglio, On the existence of a threshold for preventive behavioral responses to suppress epidemic spreading, *Sci. Rep.* **2**, 632 (2012).
- [9] A. Rizzo, M. Frasca, and M. Porfiri, Effect of individual behavior on epidemic spreading in activity-driven networks, *Phys. Rev. E* **90**, 042801 (2014).
- [10] <https://covidtracker.fr>
- [11] L. Wynants, B. Van Calster, G. S. Collins, R. D. Riley, G. Heinze, E. Schuit, E. Albu, B. Arshi, V. Bellou, M. M. Bonten *et al.*, Prediction models for diagnosis and prognosis of COVID-19: Systematic review and critical appraisal, *BMJ* **369**, m1328 (2020).
- [12] H. Salje, C. Tran Kiem, N. Lefrancq, N. Courtejoie, P. Bosetti, J. Paireau, A. Andronico, N. Hozé, J. Richet, C.-L. Dubost *et al.*, Estimating the burden of SARS-CoV-2 in France, *Science* **369**, 208 (2020).
- [13] J. Guan, Y. Wei, Y. Zhao, and F. Chen, Modeling the transmission dynamics of COVID-19 epidemic: A systematic review, *J. Biomed. Res.* **34**, 422 (2020).
- [14] Y. Huang and Q. Zhu, Game-theoretic frameworks for epidemic spreading and human decision-making: A review, *Dyn. Games Appl.* **12**, 7 (2022).
- [15] J.-M. Lasry and P.-L. Lions, Mean field games, *Jpn. J. Math.* **2**, 229 (2007).
- [16] J.-M. Lasry and P.-L. Lions, Jeux à champ moyen. II—Horizon fini et contrôle optimal, *C. R. Math.* **343**, 679 (2006).
- [17] J.-M. Lasry and P.-L. Lions, Jeux à champ moyen. I—Le cas stationnaire, *C. R. Math.* **343**, 619 (2006).
- [18] M. Huang, R. Malhame, and P. Caines, Large population stochastic dynamic games: Closed-loop McKean-Vlasov systems and the Nash certainty equivalence principle, *Commun. Inf. Syst.* **6**, 115 (2006).
- [19] P. E. Caines, Mean field games, in *Encyclopedia of Systems and Control* (Springer, Berlin, 2021).
- [20] D. A. Gomes, J. Mohr, and R. R. Souza, Continuous time finite state mean field games, *Appl. Math. Optim.* **68**, 99 (2013).

- [21] R. Carmona, F. Delarue *et al.*, *Probabilistic Theory of Mean Field Games with Applications I–II* (Springer, Berlin, 2018).
- [22] D. Ullmo, I. Swiecicki, and T. Gobron, Quadratic mean field games, *Phys. Rep.* **799**, 1 (2019).
- [23] I. Swiecicki, T. Gobron, and D. Ullmo, Schrödinger approach to mean field games, *Phys. Rev. Lett.* **116**, 128701 (2016).
- [24] A. Cousin, S. Crépey, O. Guéant, D. Hobson, M. Jeanblanc, J.-M. Lasry, J.-P. Laurent, P.-L. Lions, P. Tankov, O. Guéant *et al.*, Mean field games and applications, *Paris-Princeton Lect. Math. Fin.* **2010**, 24 (2011).
- [25] P. Chan and R. Sircar, Bertrand and Cournot mean field games, *Appl. Math. Optim.* **71**, 533 (2015).
- [26] T. Bonnemain, M. Butano, T. Bonnet, I. Echeverría-Huarte, A. Seguin, A. Nicolas, C. Appert-Rolland, and D. Ullmo, Pedestrians in static crowds are not grains, but game players, *Phys. Rev. E* **107**, 024612 (2023).
- [27] D. Bauso, R. Pesenti, and M. Tolotti, Opinion dynamics and stubbornness via multi-population mean-field games, *J. Optim. Theory Appl.* **170**, 266 (2016).
- [28] T. C. Reluga, Game theory of social distancing in response to an epidemic, *PLoS Comput. Biol.* **6**, e1000793 (2010).
- [29] L. Laguzet, G. Turinici, and G. Yahiaoui, Equilibrium in an individual-societal SIR vaccination model in presence of discounting and finite vaccination capacity, in *New Trends in Differential Equations, Control Theory and Optimization: Proceedings of the 8th Congress of Romanian Mathematicians* (World Scientific, Singapore, 2016).
- [30] E. Hubert and G. Turinici, Nash-MFG equilibrium in a SIR model with time dependent newborn vaccination, *Ric. Mat.* **67**, 227 (2018).
- [31] F. Salvarani and G. Turinici, Optimal individual strategies for influenza vaccines with imperfect efficacy and durability of protection, *Math. Biosci. Eng.* **15**, 629 (2018).
- [32] R. Elie, E. Hubert, and G. Turinici, Contact rate epidemic control of COVID-19: An equilibrium view, *Math. Modell. Nat. Phenom.* **15**, 35 (2020).
- [33] S. Y. Olmez, S. Aggarwal, J. W. Kim, E. Miehl, T. Başar, M. West, and P. G. Mehta, Modeling presymptomatic spread in epidemics via mean-field games, in *Proceedings of the American Control Conference (ACC)* (IEEE, Piscataway, NJ, 2022).
- [34] S. Y. Olmez, S. Aggarwal, J. W. Kim, E. Miehl, T. Başar, M. West, and P. G. Mehta, How does a rational agent act in an epidemic?, in *Proceedings of the IEEE 61st Conference on Decision and Control (CDC)* (IEEE, Piscataway, NJ, 2022).
- [35] A. Roy, C. Singh, and Y. Narahari, Recent advances in modeling and control of epidemics using a mean field approach, *Sādhanā* **48**, 207 (2023).
- [36] W. O. Kermack and A. G. McKendrick, A contribution to the mathematical theory of epidemics, *Proc. R. Soc. London, Ser. A* **115**, 772 (1927).
- [37] H. W. Hethcote, The mathematics of infectious diseases, *SIAM Rev.* **42**, 599 (2000).
- [38] L. Fumanelli, M. Ajelli, P. Manfredi, A. Vespignani, and S. Merler, Inferring the structure of social contacts from demographic data in the analysis of infectious diseases spread, *PLoS Comput. Biol.* **8**, e1002673 (2012).
- [39] D. Mistry, M. Litvinova, A. Pastore y Piontti, M. Chinazzi, L. Fumanelli, M. F. Gomes, S. A. Haque, Q.-H. Liu, K. Mu, X. Xiong *et al.*, Inferring high-resolution human mixing patterns for disease modeling, *Nat. Commun.* **12**, 323 (2021).
- [40] S. Merler, M. Ajelli, A. Pugliese, and N. M. Ferguson, Determinants of the spatiotemporal dynamics of the 2009 H1N1 pandemic in Europe: Implications for real-time modelling, *PLoS Comput. Biol.* **7**, e1002205 (2011).
- [41] S. Eubank, H. Guclu, V. Anil Kumar, M. V. Marathe, A. Srinivasan, Z. Toroczkai, and N. Wang, Modelling disease outbreaks in realistic urban social networks, *Nature (London)* **429**, 180 (2004).
- [42] R. Dutta, S. N. Gomes, D. Kalise, and L. Pacchiardi, Using mobility data in the design of optimal lockdown strategies for the COVID-19 pandemic, *PLoS Comput. Biol.* **17**, e1009236 (2021).
- [43] D. Sen and D. Sen, Use of a modified SIRD model to analyze COVID-19 data, *Ind. Eng. Chem. Res.* **60**, 4251 (2021).
- [44] S. Gao, Z. Teng, J. J. Nieto, A. Torres *et al.*, Analysis of an SIR epidemic model with pulse vaccination and distributed time delay, *Biomed Res. Int.* **2017**, 064870 (2007).
- [45] H. Li and S. Guo, Dynamics of a SIRC epidemiological model, *Electron. J. Differ. Equations* **2017**, 1 (2017).
- [46] M. Y. Li, H. L. Smith, and L. Wang, Global dynamics of an SEIR epidemic model with vertical transmission, *SIAM J. Appl. Math.* **62**, 58 (2001).
- [47] A. Arenas, W. Cota, J. Gómez-Gardeñes, S. Gómez, C. Granell, J. T. Matamalas, D. Soriano-Paños, and B. Steinegger, Modeling the spatiotemporal epidemic spreading of COVID-19 and the impact of mobility and social distancing interventions, *Phys. Rev. X* **10**, 041055 (2020).
- [48] S. Y. Del Valle, J. M. Hyman, H. W. Hethcote, and S. G. Eubank, Mixing patterns between age groups in social networks, *Soc. Netw.* **29**, 539 (2007).
- [49] G. Béraud, S. Kazmerczak, P. Beutels, D. Levy-Bruhl, X. Lenne, N. Mielcarek, Y. Yazdanpanah, P.-Y. Boëlle, N. Hens, and B. Dervaux, The french connection: The first large population-based contact survey in france relevant for the spread of infectious diseases, *PLoS ONE* **10**, e0133203 (2015).
- [50] L. Di Domenico, G. Pullano, C. E. Sabbatini, P.-Y. Boëlle, and V. Colizza, Impact of lockdown on COVID-19 epidemic in île-de-france and possible exit strategies, *BMC Med.* **18**, 240 (2020).
- [51] J. Tchuenche, S. Khamis, F. Agosto, and S. Mpeshe, Optimal control and sensitivity analysis of an influenza model with treatment and vaccination, *Acta Biotheor.* **59**, 1 (2011).
- [52] D. Bertsekas, *Dynamic Programming and Optimal Control: Volume I* (Athena Scientific, Nashua, NH, 2012), Vol. 4.
- [53] A. Abakuks, An optimal isolation policy for an epidemic, *J. Appl. Probab.* **10**, 247 (1973).
- [54] A. Abakuks, Optimal immunisation policies for epidemics, *Adv. Appl. Probab.* **6**, 494 (1974).
- [55] M. Kantner and T. Koprucki, Beyond just “flattening the curve”: Optimal control of epidemics with purely nonpharmaceutical interventions, *J. Math. Ind.* **10**, 23 (2020).
- [56] T. Kruse and P. Strack, Optimal control of an epidemic through social distancing, SSRN (2020), <http://dx.doi.org/10.2139/ssrn.3581295>.
- [57] M. Khouzani, S. Sarkar, and E. Altman, Optimal control of epidemic evolution, in *Proceedings of the IEEE INFOCOM* (IEEE, Piscataway, NJ, 2011).
- [58] Our criterion is actually better suited to describe herd immunity at the end of the epidemics than, for instance, the one which requires $S < 1/\tilde{R}_0$ with $\tilde{R}_0 = \rho(\rho\mu\mathcal{M}/\xi)$ [38,60].

- [59] A. Aurell, R. Carmona, G. Dayanikli, and M. Lauriere, Optimal incentives to mitigate epidemics: A Stackelberg mean field game approach, *SIAM J. Control Optim.* **60**, S294 (2022).
- [60] O. Diekmann, J. A. P. Heesterbeek, and J. A. J. Metz, On the definition and the computation of the basic reproduction ratio R_0 in models for infectious diseases in heterogeneous populations, *J. Math. Biol.* **28**, 365 (1990).